4 Microstructural investigation

As mentioned in a previous section, a clear appreciation of the microstructure is critical for understanding the observed kinetic behaviour. It is therefore prudent to examine closely the key graphite samples used in this study. Firstly, the nuclear-grade natural graphite sample, NNG, will be discussed. An SEM image of the as-received material is shown in Figure 4-1.

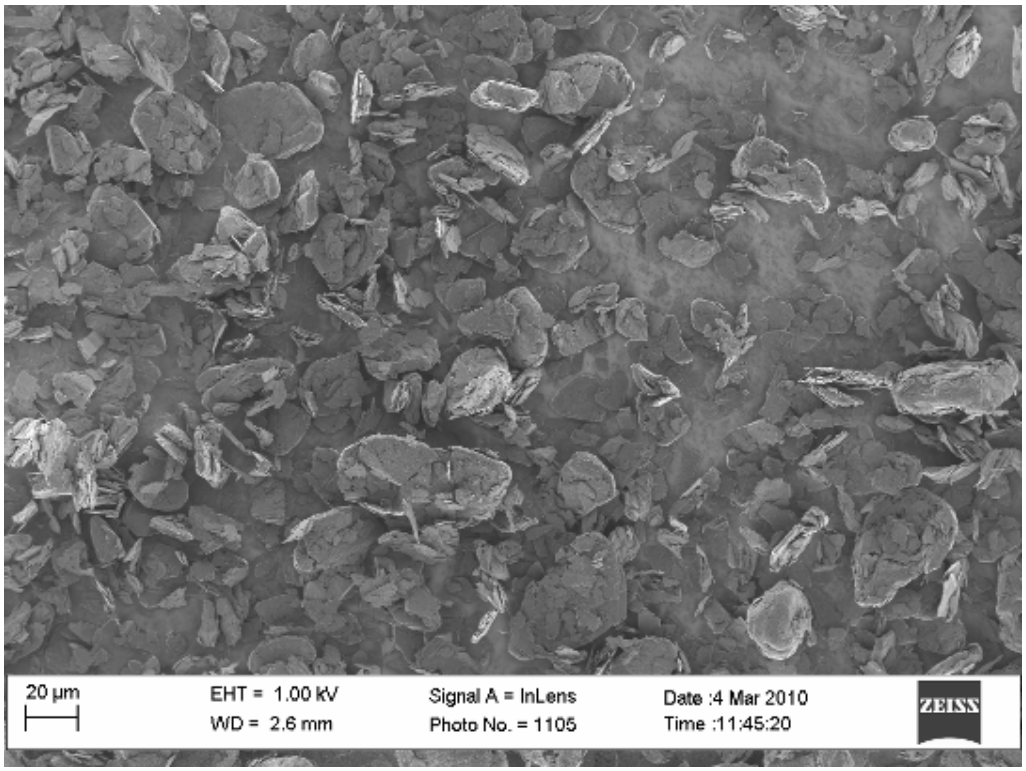

Figure 4-1: SEM of as-received NNG graphite (750x magnification)

At first glance it is clear that a wide spread of particle sizes are present, despite the fairly narrow PSD shown in Figure 3-9. It also appears that a large portion of the particles are smaller than the 22 µm average diameter determined from the PSD. Upon closer inspection, the particles appear to be highly agglomerated, as can be seen from Figure 4-2, with smaller particles adhering to larger ones.

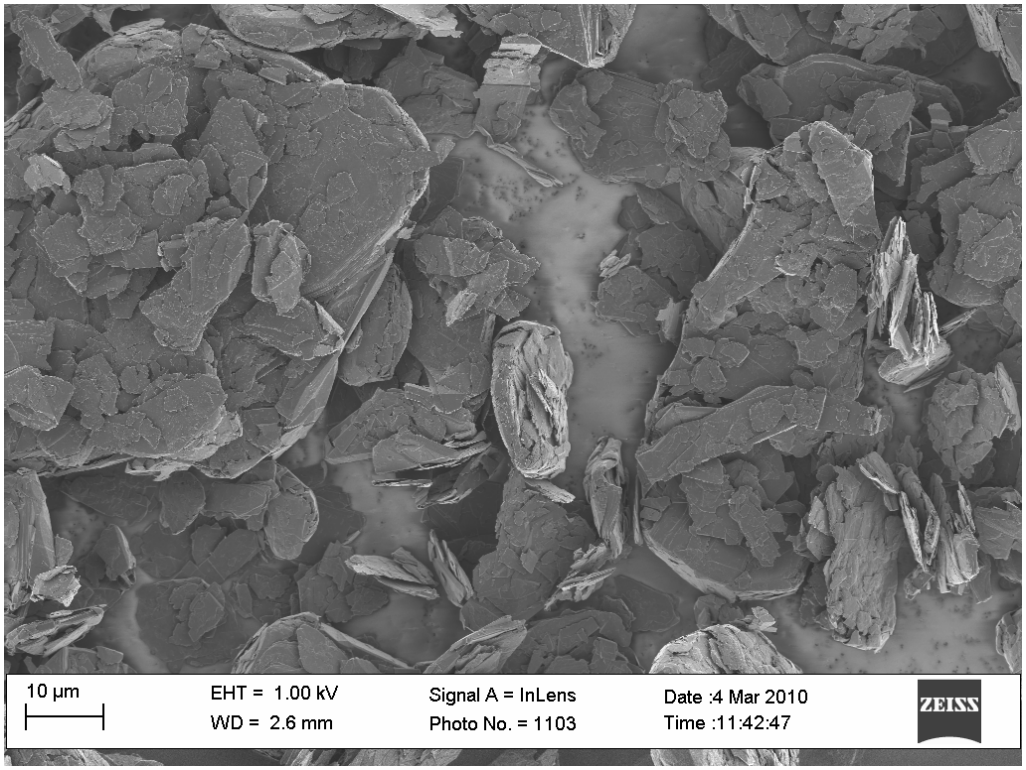

Figure 4-2: SEM of as-received NNG graphite (2 000x magnification)

However, when the larger particles are examined at higher magnification as in Figure 4-3, the layered structure characteristic of graphite is clearly visible. The flakes seem to be highly crystalline with little or no porosity, as can be seen in Figure 4-4.

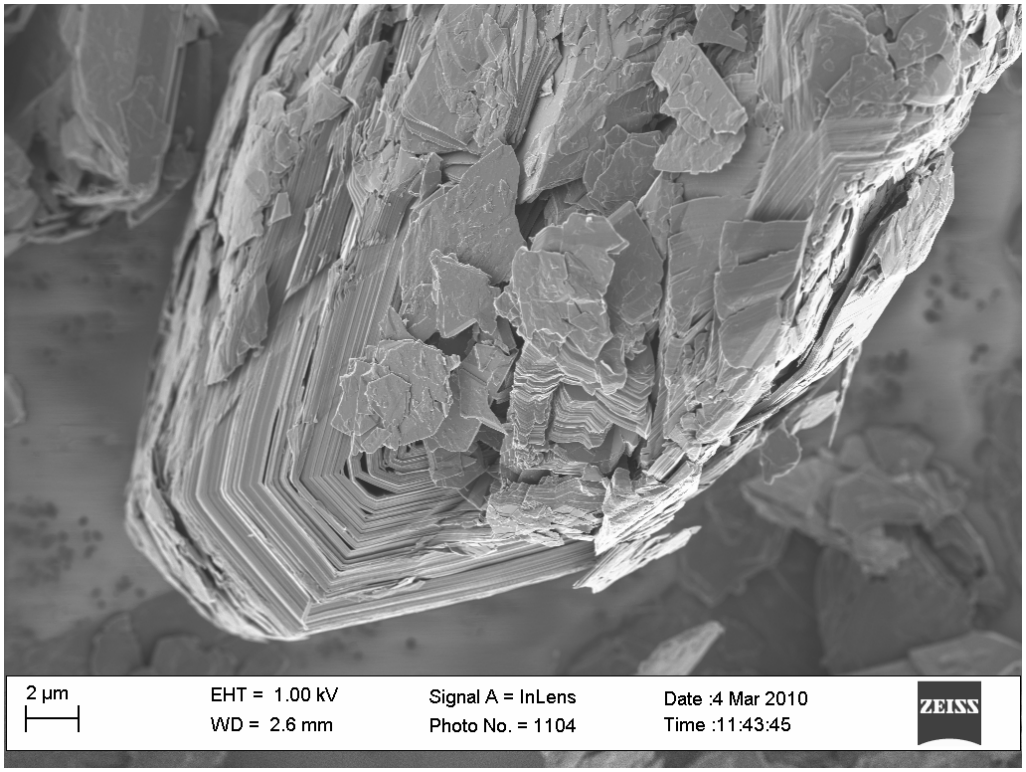

Figure 4-3: SEM of NNG graphite flake (8 000x magnification)

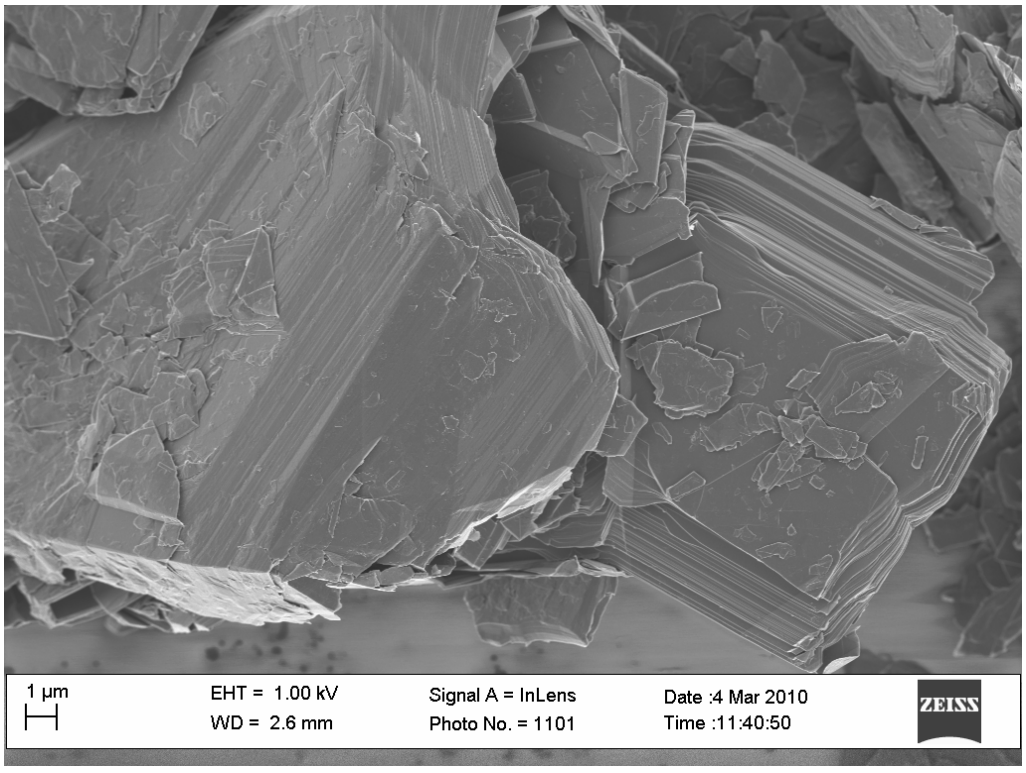

Figure 4-4: SEM of NNG graphite flakes (9 000x magnification)

Modelling the microstructural evolution of such a wide mixture of particle sizes would be difficult. Instead, it would be easier to obtain single flakes of a certain size range. However, the tendency of the graphite to agglomerate makes this difficult. It was found that using ethanol as a solvent broke up the agglomerates and allowed a much narrower particle size distribution of clean single flakes to be obtained, as shown in Figure 4-5. Other solvents were also assessed but these, especially acetone, tended to leave clearly visible residues on the flakes. Only ethanol evaporated completely whilest still effectively breaking up the agglomeration.

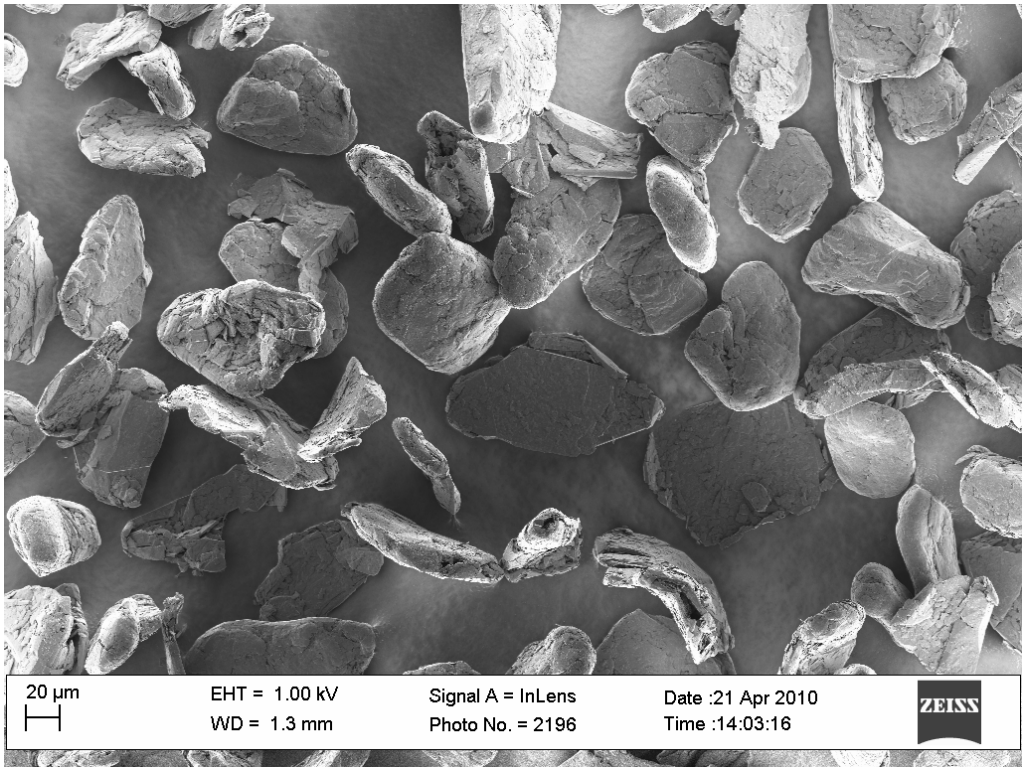

Figure 4-5: SEM of ethanol-washed NNG graphite flakes (500x magnification)

However, when these flakes are examined more closely, they still appear to be agglomerates of very fine particles, as can be seen in Figure 4-6.

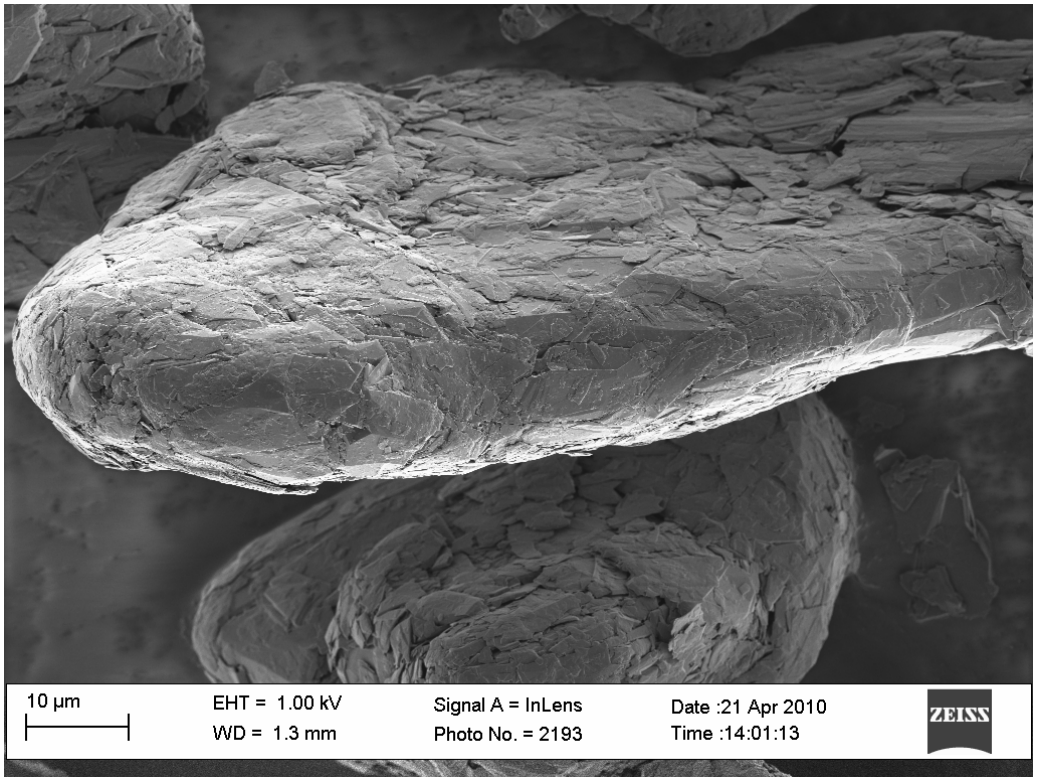

Figure 4-6: SEM of ethanol-washed NNG graphite flake (3 000x magnification)

Further examination of the flakes led to the discovery of flakes with clearly damaged edge structures, as shown in Figure 4-7 and Figure 4-8. The edges of these flakes are curled back towards the centre of the flake and the edge is severely roughened. Initially, these flakes were sonicated in a water bath for 5 min while being contained in a test tube with ethanol. This was to ensure separation of the agglomerates. Clearly, the flakes are highly malleable and damage easily.

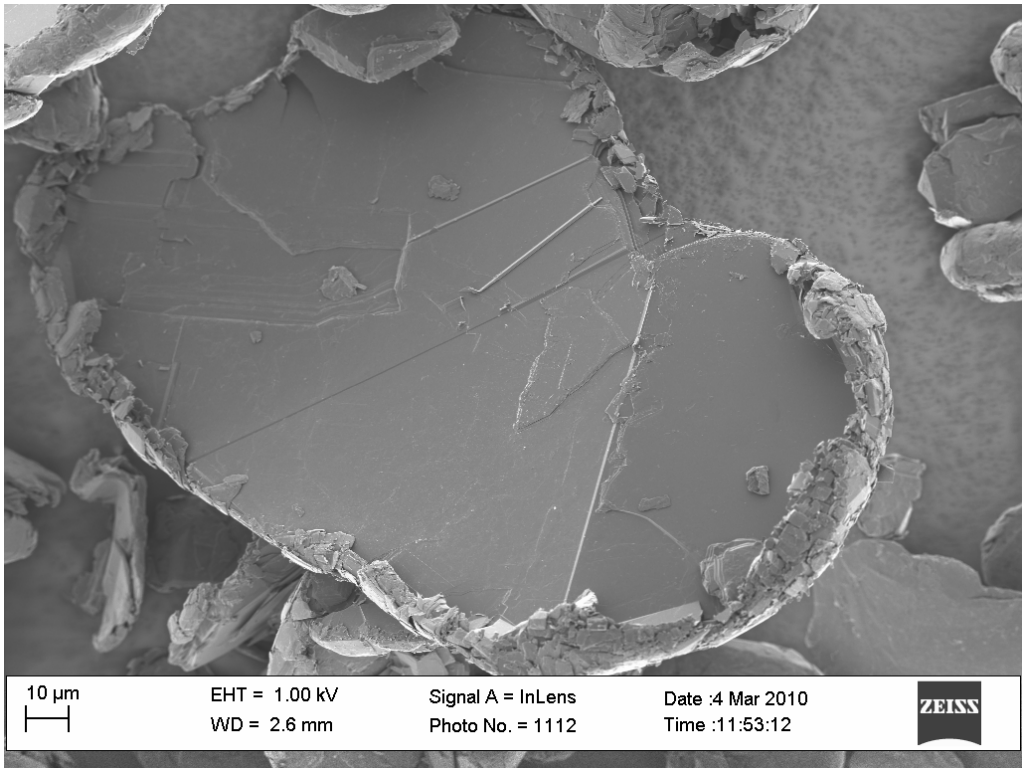

Figure 4-7: SEM of damaged NNG graphite flake (1 000x magnification)

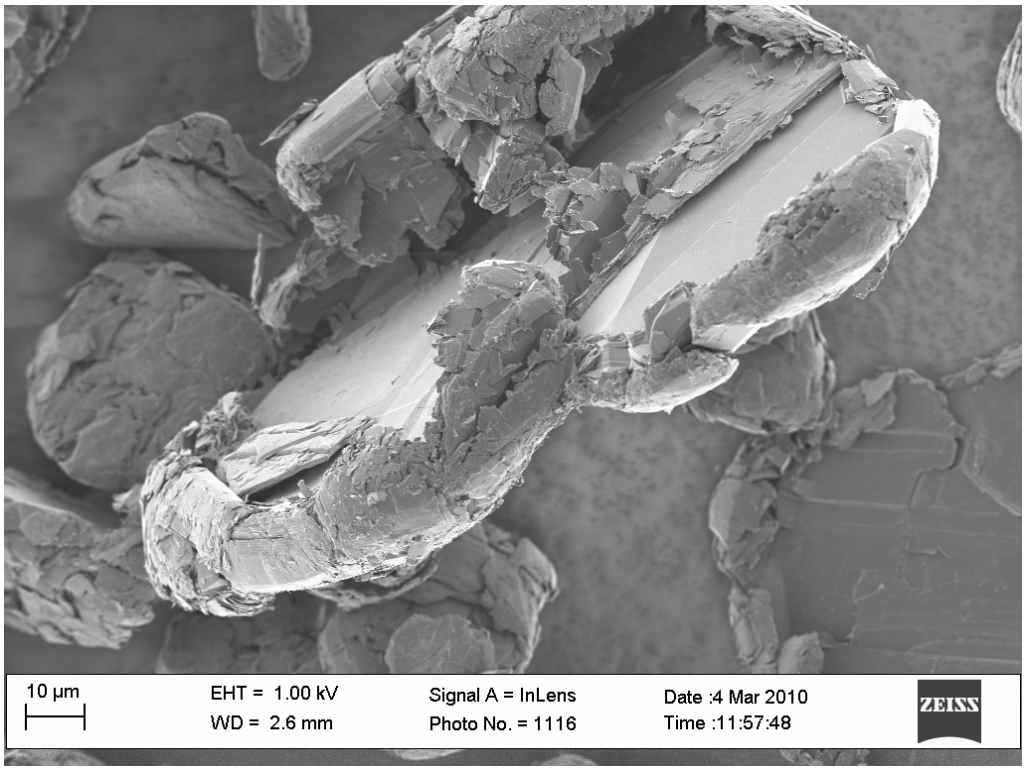

Figure 4-8: SEM of damaged NNG graphite flake (2 000x magnification)

It was concluded that the NNG sample had undergone extensive milling, probably in a jet mill, at some point during its production. This is a known treatment for obtaining the so-called “potato-shaped” particles, as can be seen in Figure 4-9.

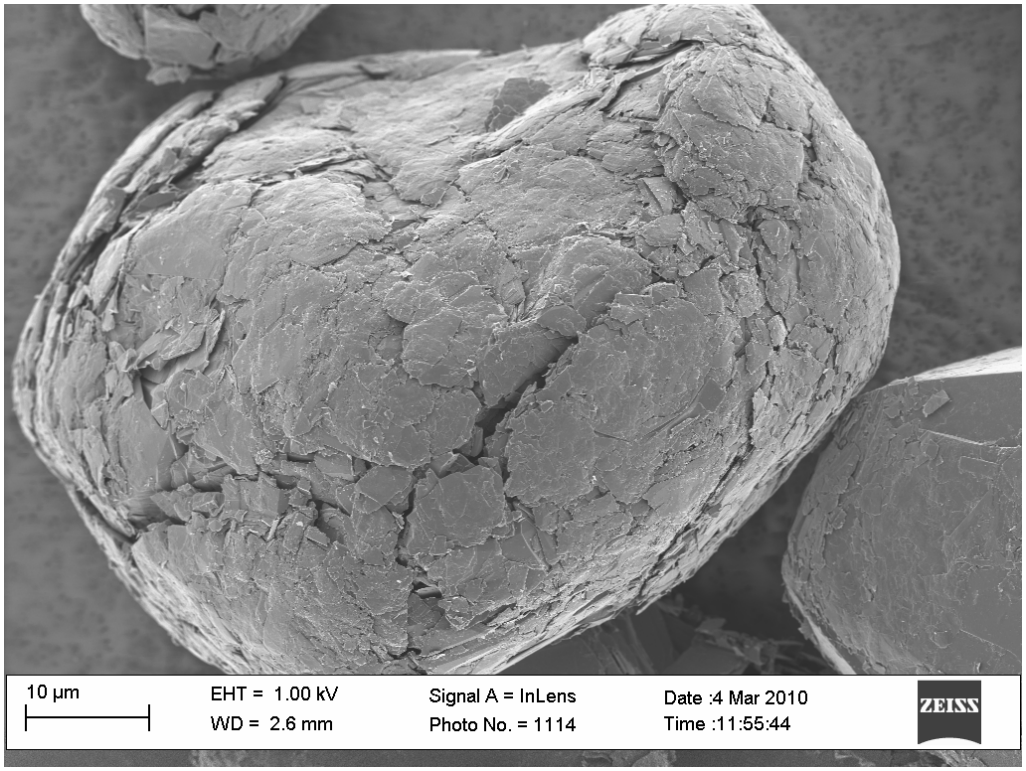

Figure 4-9: SEM of potato-shaped NNG graphite flake (4 000x magnification)

The particles are therefore so extensively damaged that they appear to be agglomerates. It is clear that the microstructural development of such a particle would be extremely difficult to simulate. Thus this sample is not ideally suited to fundamental modelling. The second sample that was considered is the nuclear-grade synthetic graphite (NSG), which is shown as-received in Figure 4-10.

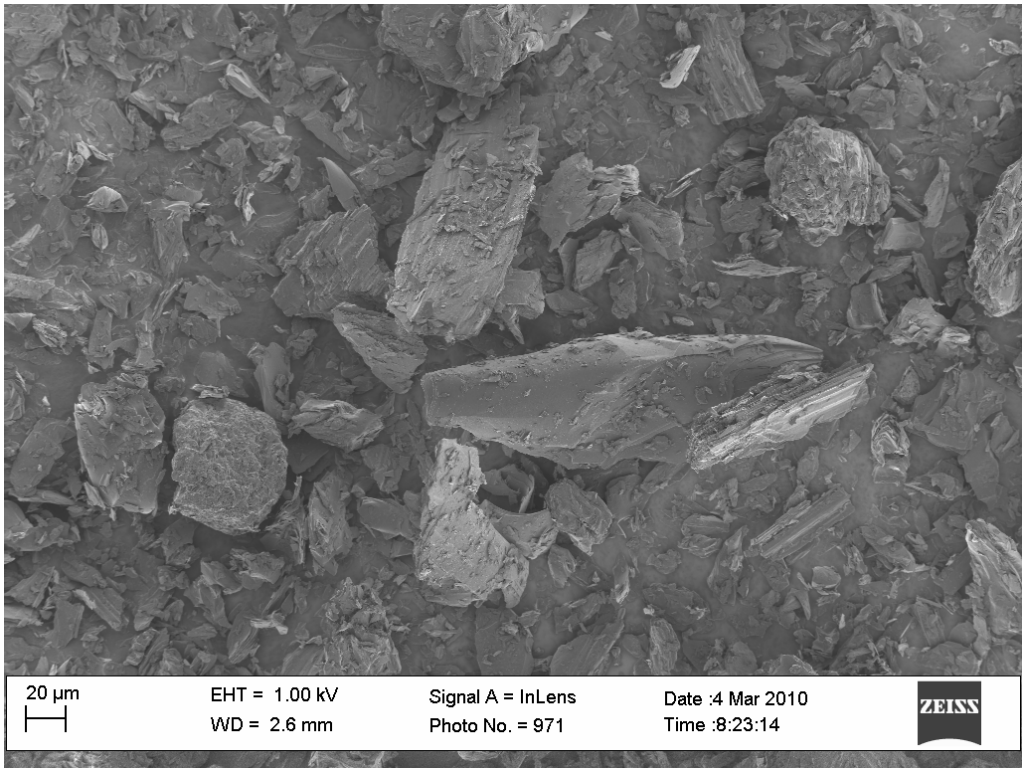

Figure 4-10: SEM of as-received NSG graphite (600x magnification)

This sample also has a mixture of large and small particles, but apparently with a lesser tendency to agglomerate. The sample was washed in ethanol, with care being taken to avoid damage to the structure to obtain the clean flakes shown in Figure 4-11.

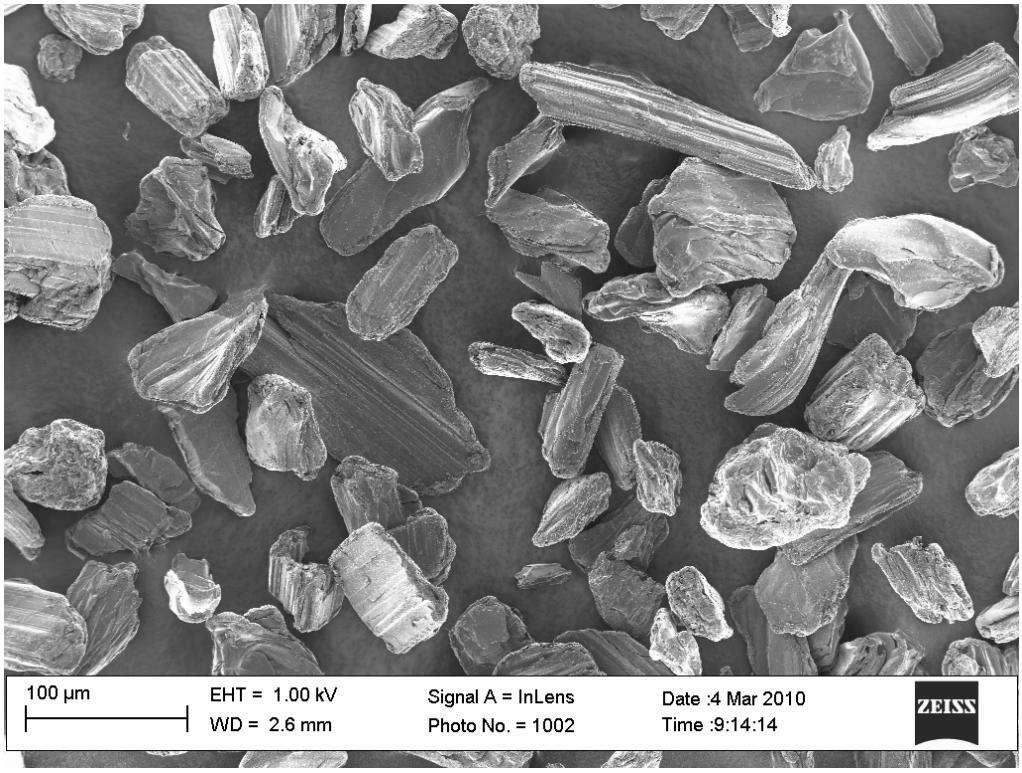

Figure 4-11: SEM of ethanol-washed NSG graphite (500x magnification)

The long, rod-like particles are immediately discernible. These particles are derived from the needle coke precursor used to produce synthetic graphite, as discussed in Section 2.3.3. When examined more closely, their layered graphitic structure can be clearly seen, as in Figure 4-12.

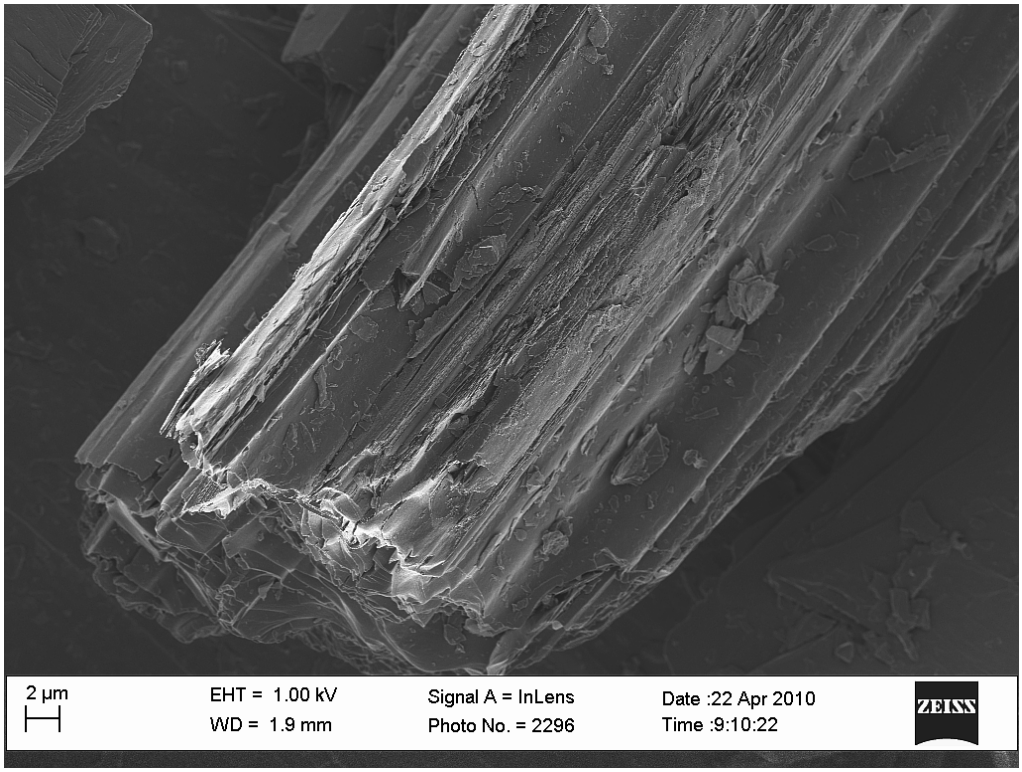

Figure 4-12: SEM of NSG needle coke particle (5 000x magnification)

However, when the particles are examined edge-on, their complex microstructure is noticeable. They have the appearance of sheets of paper that have been erratically rolled and crumpled along their long axis. Hence they have long slit-shaped pores running into the particle, as can be seen from Figure 4-13.

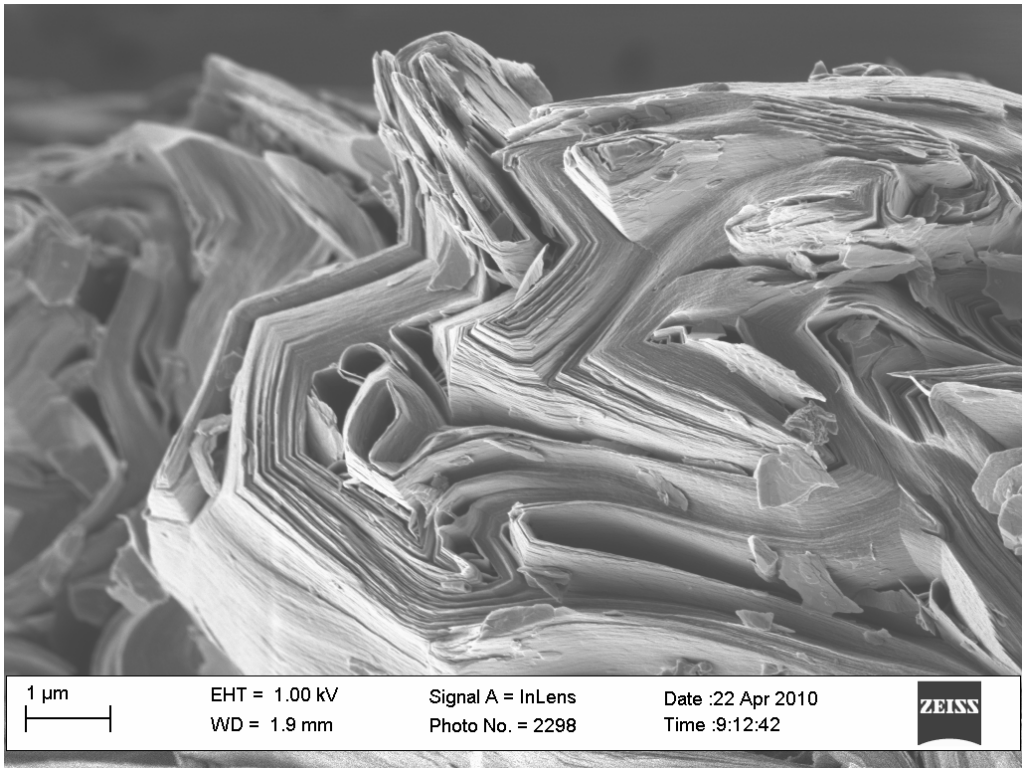

Figure 4-13: SEM of NSG needle coke particle edge-on (25 000x magnification)

A second type of particle is readily distinguishable and is shown in Figure 4-14. This particle has an exceedingly complex microstructure with a characteristic flow or mosaic texture, as can be seen in more detail in Figure 4-15. These particles are most likely derived from regions in the bulk material where pitch was impregnated. This led to the characteristic wave-like patterns in the particle microstructure, which occurred as the liquid pitch material solidified.

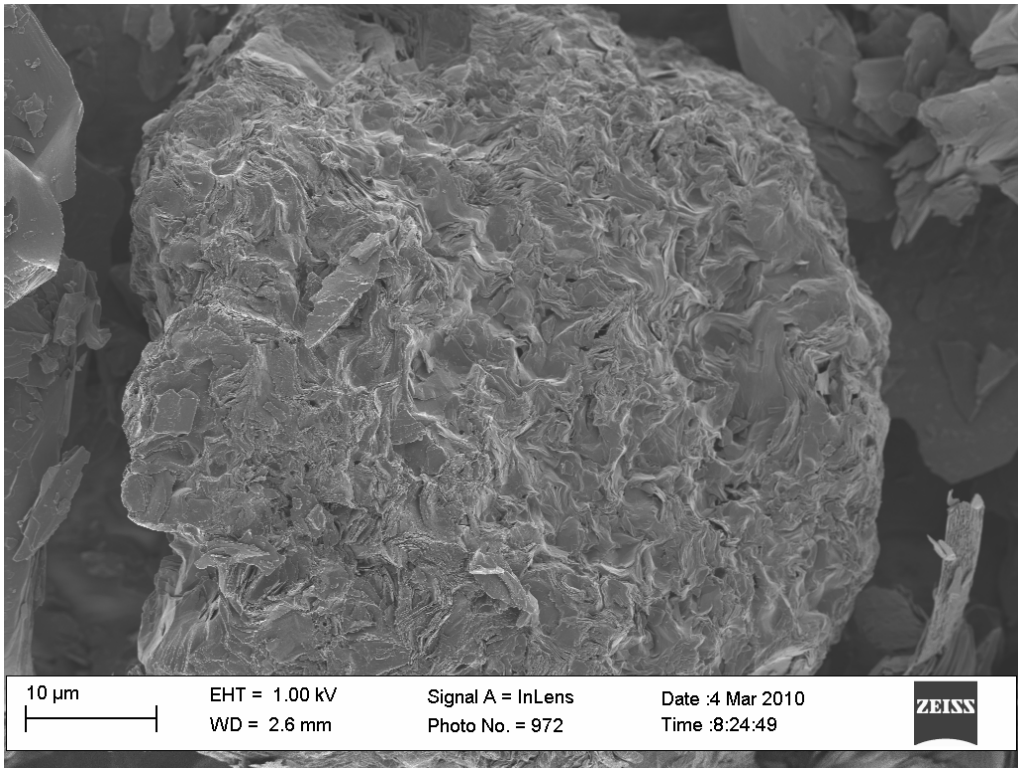

Figure 4-14: SEM of NSG pitch particle (4 000x magnification)

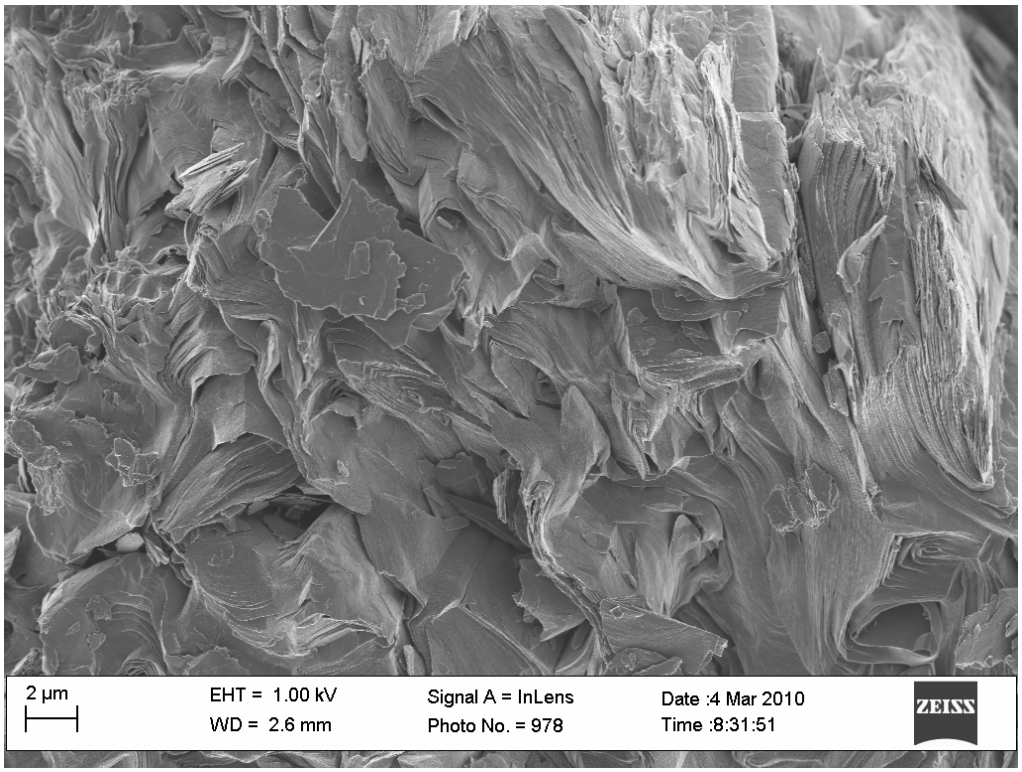

Figure 4-15: SEM of NSG flow domain (8 000x magnification)

When these particles are oxidised, extremely complex microstructures arise with a high degree of porosity, as shown in Figure 4-16 and Figure 4-17.

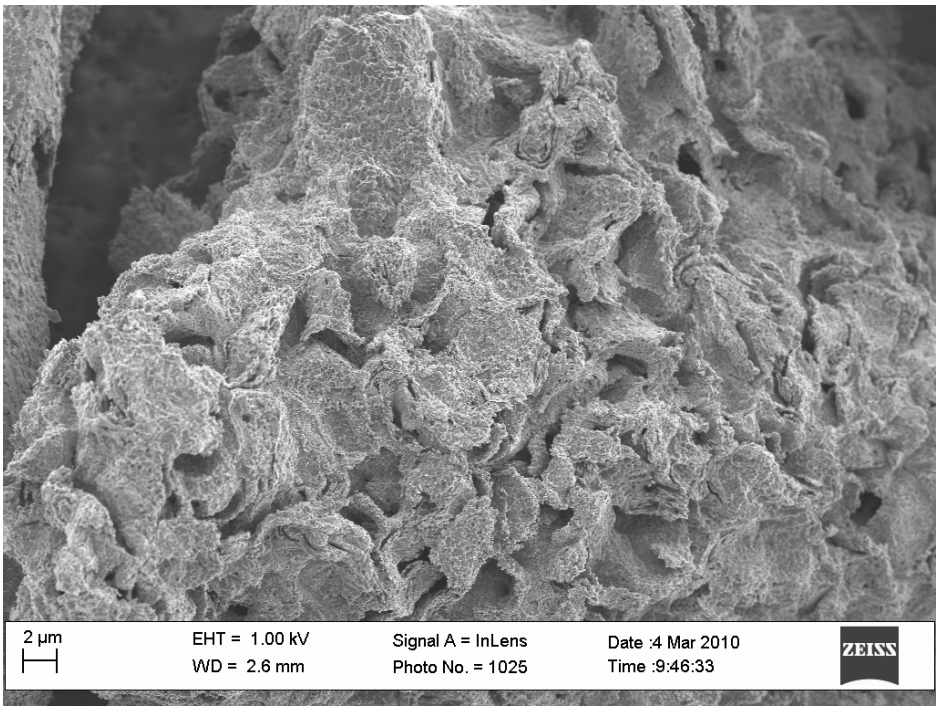

Figure 4-16: SEM of oxidised NSG pitch particle (5 000x magnification)

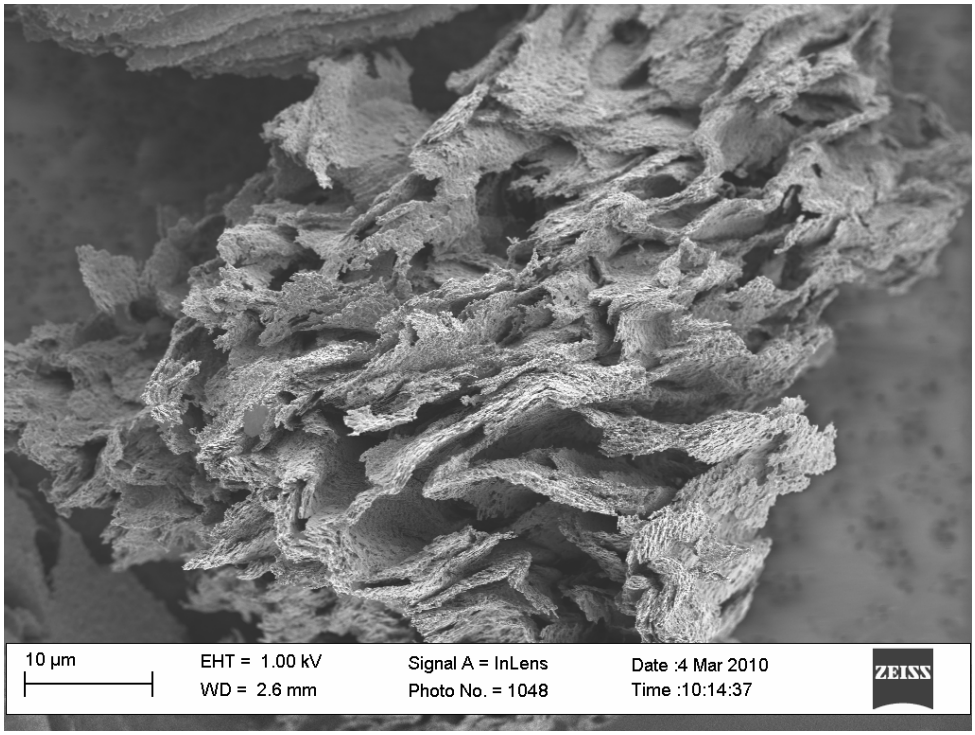

Figure 4-17: SEM of oxidised NSG pitch particle (4 000x magnification)

The characteristic layered structure of the synthetic graphite is, however, easily discernible in the oxidised particles, as can be seen in Figure 4-18. However, it is still unclear how the crystallinity of the two samples compares.

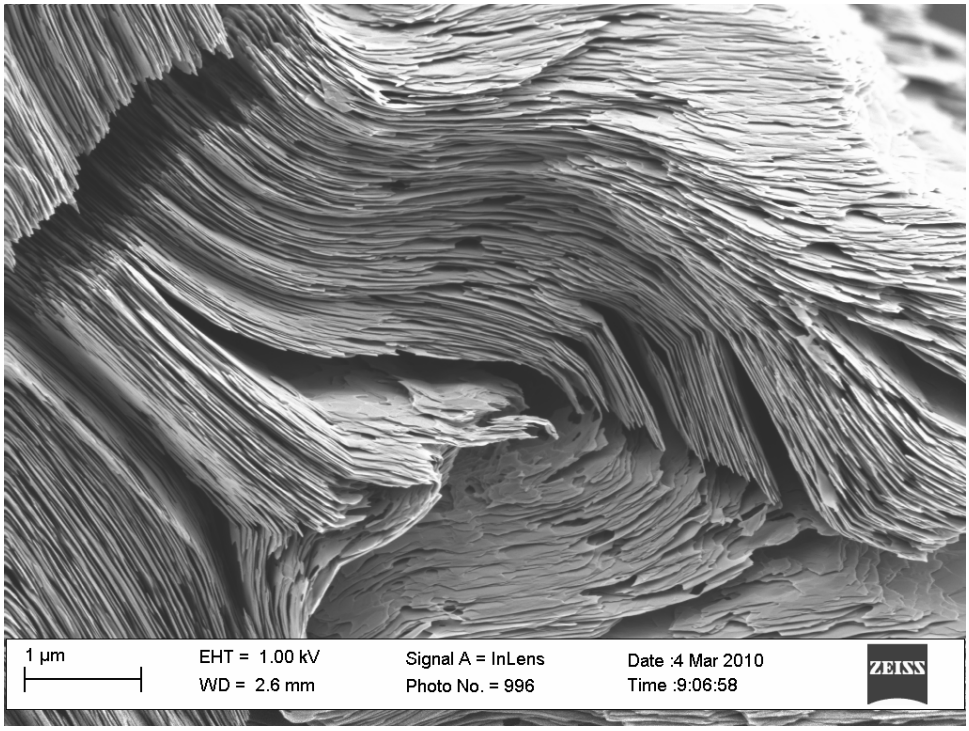

Figure 4-18: SEM of NSG layered structure (35 000x magnification)

Using the XRD data and the Scherrer equation, Eq. (2.4), the domain sizes, i.e. crystallite height (L_c) and radius (L_a), of the two graphite samples just examined can be determined. In addition, using the method of Tuinstra and Koenig [47] given by Eq. (2.5) and the Raman spectra, the crystallite radius can be determined. These values are given in Table 4-1.

Table 4-1: Crystallite domain sizes

	XRD		**Raman**
	L_c (nm)	L_a (nm)	L_a (nm)
NNG	37	38	24
NSG	38	27	38

The XRD and Raman results for the crystallite radius are contradictory, but the values are very much of the same order of magnitude. The values would indicate that the crystallinity of the natural and synthetic materials should be very similar. However, when the oxidised samples are compared, this is found not to be the case. Firstly, consider the basal and edge structures of an oxidised NNG flake shown in Figure 4-19 and Figure 4-20 respectively.

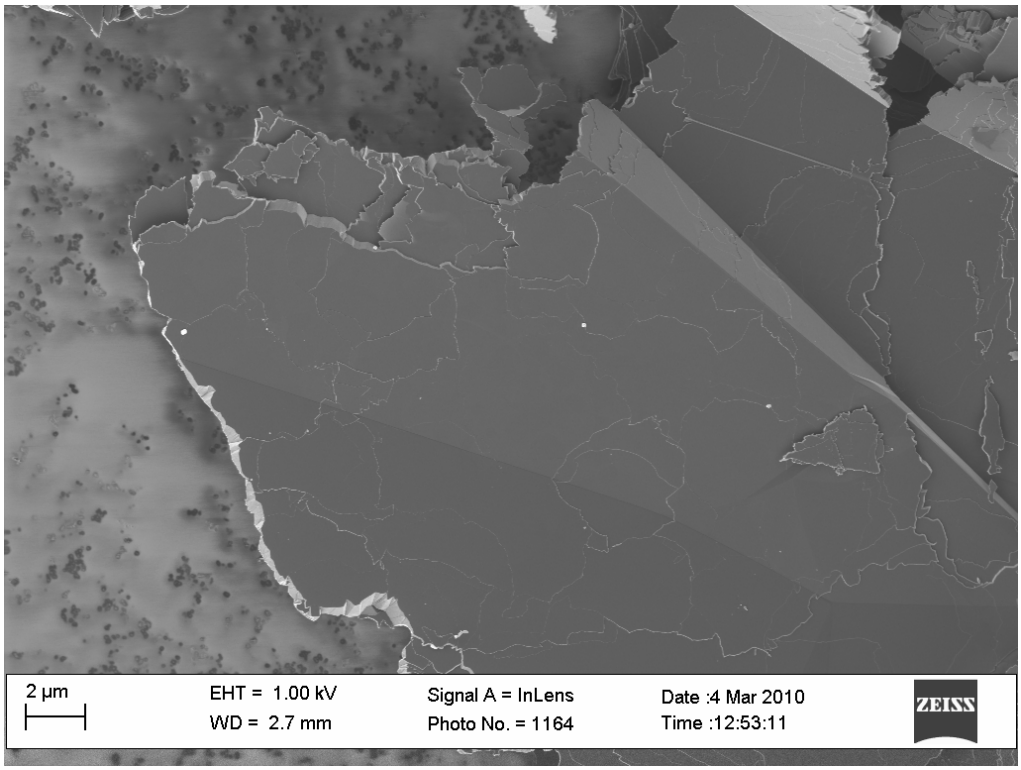

Figure 4-19: Oxidised NNG flake basal plane (9 000x magnification)

The basal plane is almost perfectly intact over extremely large distances, between 10 and 20 µm. This indicates that the entire flake is highly crystalline and cannot be attacked from this direction. Furthermore, the edge is fairly smooth and evenly oxidised in layers up to a few micron, as can be noticed when examining the flake edge-on in Figure 4-20. Visually, the flakes seem to have far larger crystalline domains than predicted by either XRD or Raman. The situation is vastly different for the synthetic graphite flakes, as can be seen in Figure 4-21 and Figure 4-22.

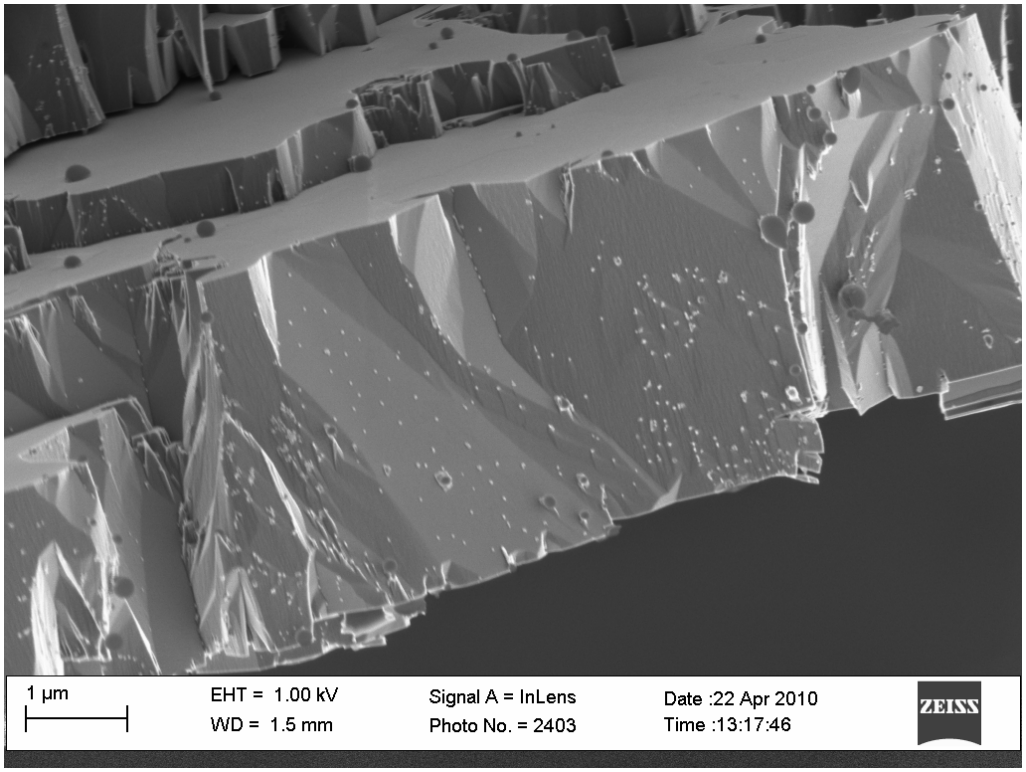

Figure 4-20: Oxidised NNG flake edge (30 000x magnification)

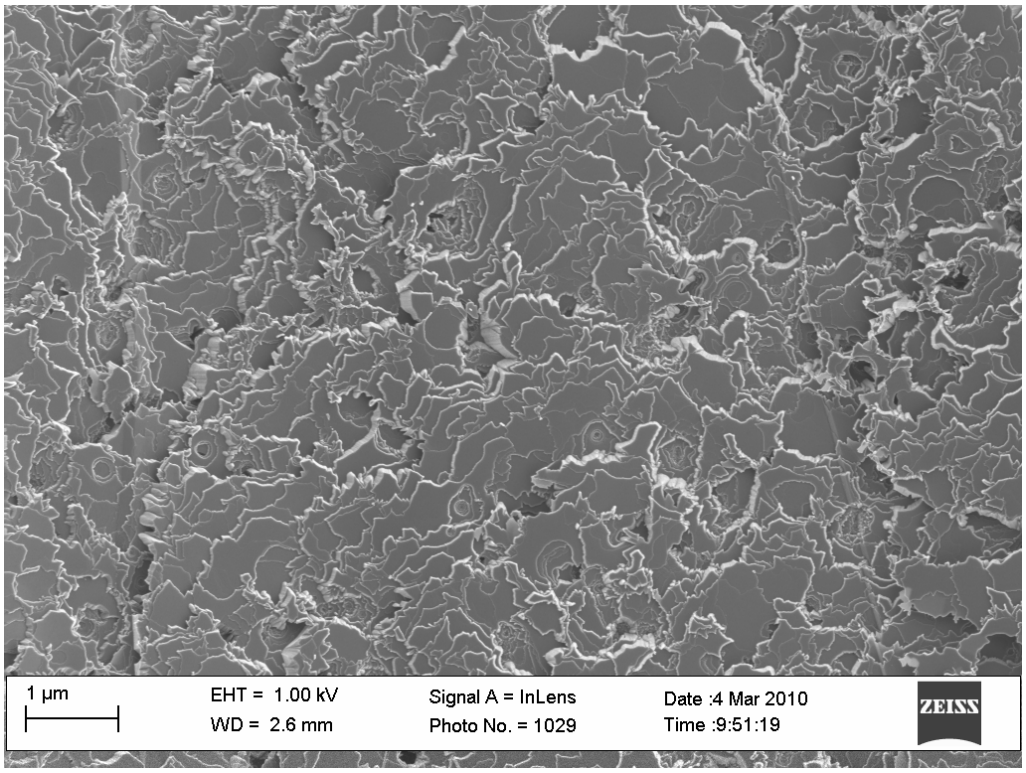

Figure 4-21: Oxidised NSG particle basal plane (28 000x magnification)

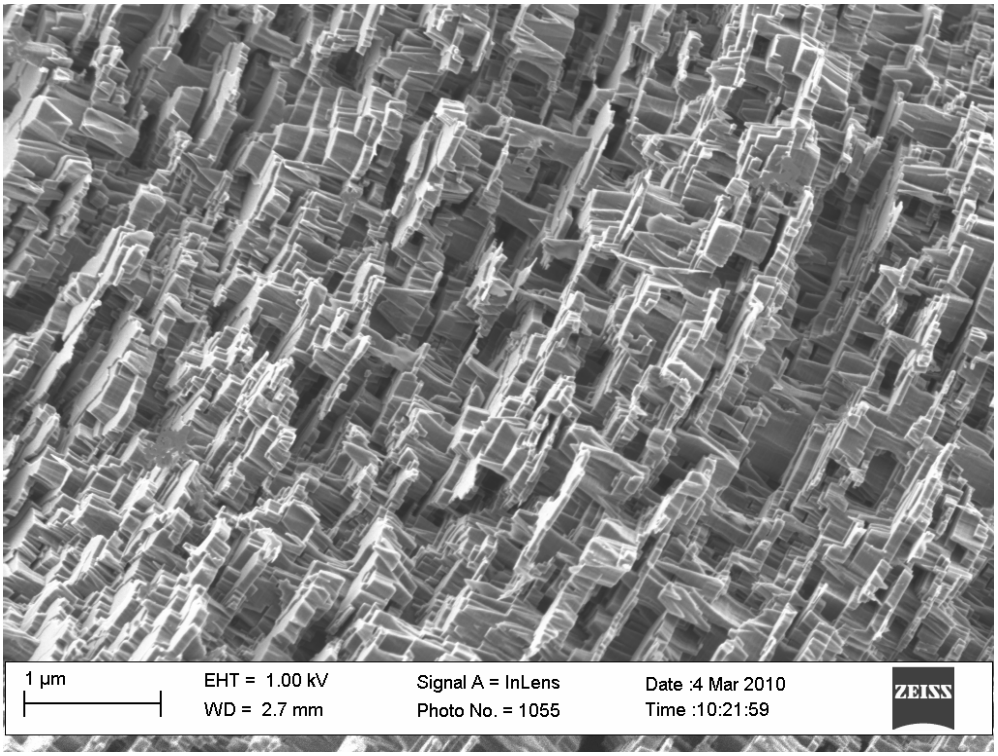

Figure 4-22: Oxidised NSG particle edge (41 000x magnification)

In this case the basal planes are severely damaged and roughened. The basal plane can be readily attacked on intervals below 100 nm and the edge shows a very finely textured structure with intact regions of the same order of magnitude. This is what is to be expected from the domain sizes calculated earlier to be around 30–40 nm. However, this does illustrate the dangers of using the XRD and Raman data to infer the extent of crystallinity. The natural graphite sample is clearly far more crystalline than the synthetic sample and behaves as would be expected for a perfectly crystalline flake of graphite.

The low degree of crystallinity, combined with the already complex microstructures mentioned earlier, leads to the development of some very intricate and erratic structures, such as those in Figure 4-23. The porosity development of these structures is also unique in the sense that as oxidation proceeds, slit-like pores arise, as can be seen in Figure 4-24. These pores are parallel to the basal plane and may lead to the development of mass transfer limitations along these narrow channels.

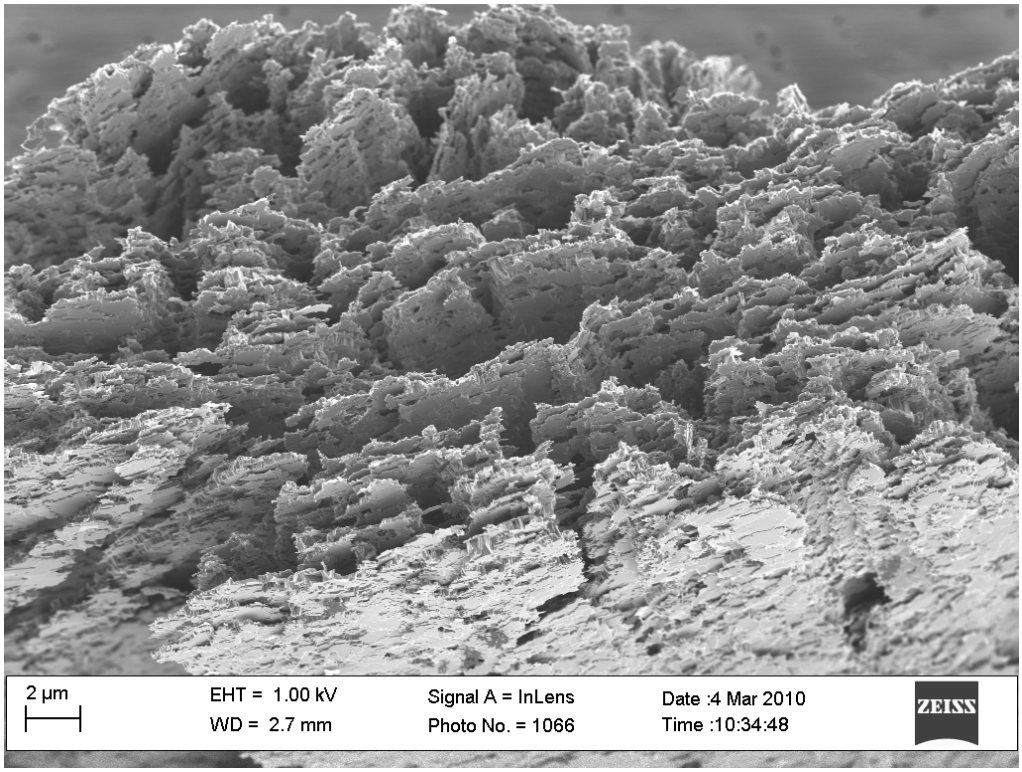

Figure 4-23: Complex NSG structural development (8 000x magnification)

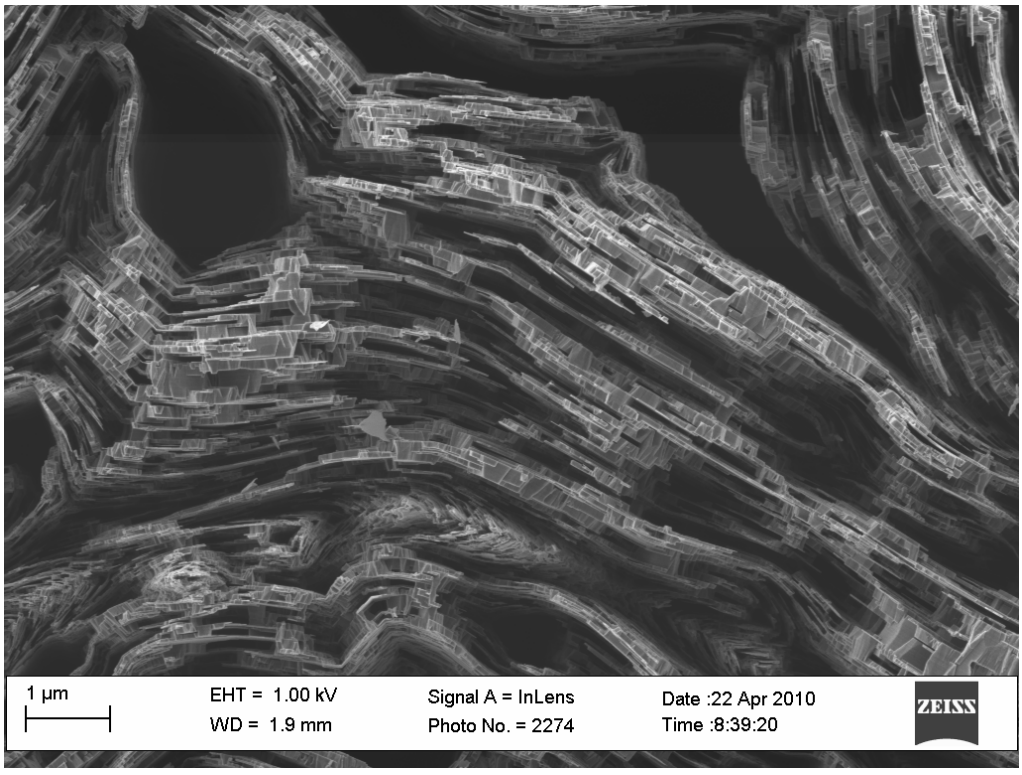

Figure 4-24: NSG pore development (41 000x magnification)

Synthetic graphite therefore represents a particularly troublesome material since such small domains would in effect imply an, at least partially, amorphous structure, similar to the structures considered in Section 2.4. These factors make it difficult to simulate the development of the microstructure taking place in the synthetic graphite sample. From a fundamental modelling perspective, this sample is not suitable for developing a mechanistic understanding of the oxidation process. In a certain sense, the large highly crystalline Kish graphite flakes, shown in Figure 4-25, are the ideal starting material.

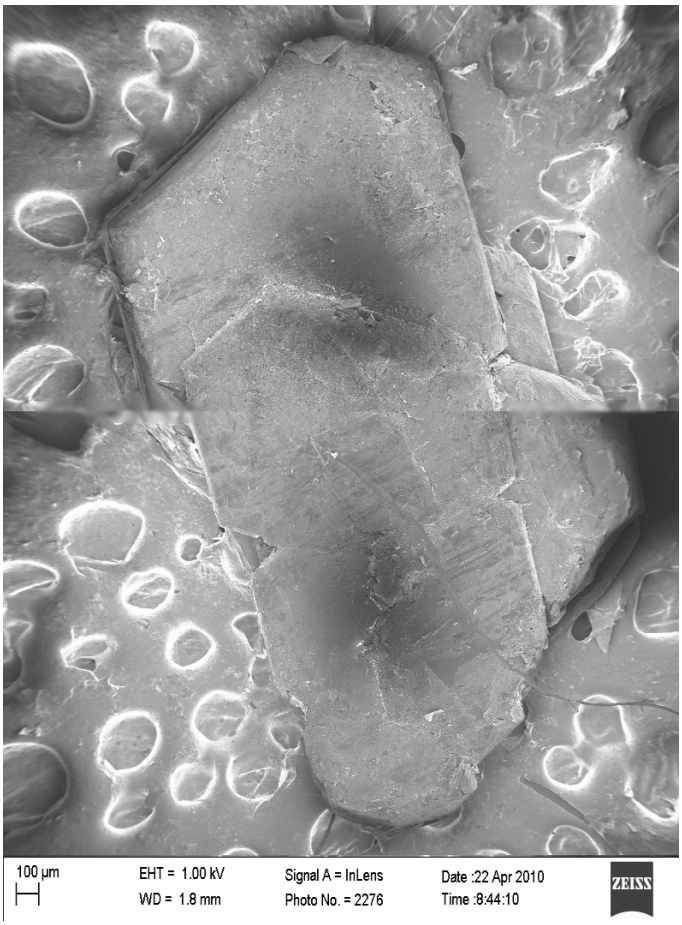

Figure 4-25: Single Kish graphite flake (100x magnification)

The layered, graphitic nature of the flake is immediately evident and the edge structures are characterised by 120º angles, as can be seen in Figure 4-26. This is to be expected for highly crystalline material due to the hexagonal crystal lattice. However, the particle shapes are not all the same and therefore the

structural development for each specific shape will be different from the next. This is further complicated by the development of discrete pits in the flake during oxidation, as can be seen in Figure 4-27.

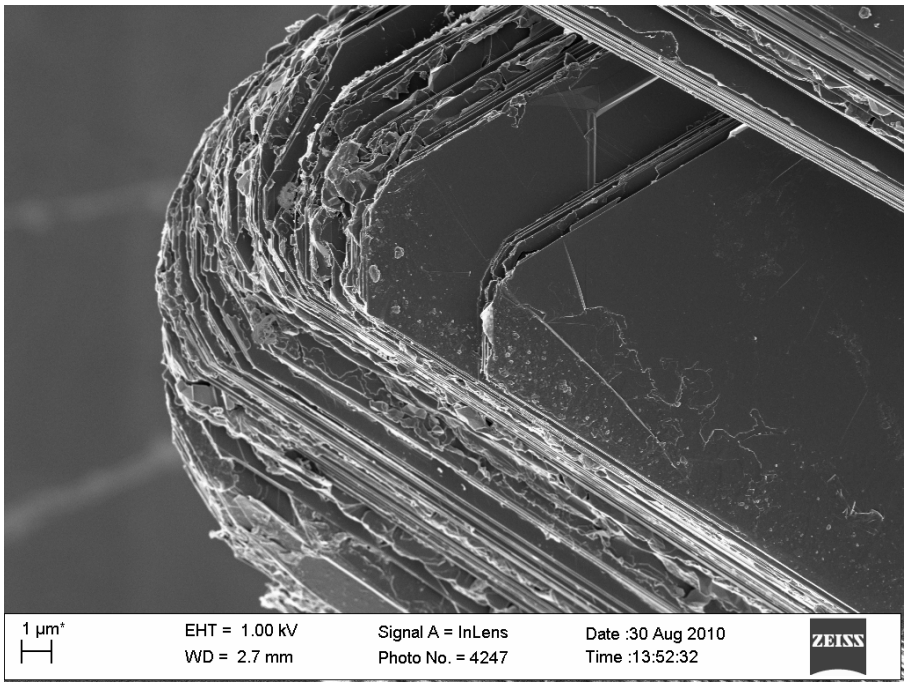

Figure 4-26: Edge structure of Kish graphite (10 000x magnification)

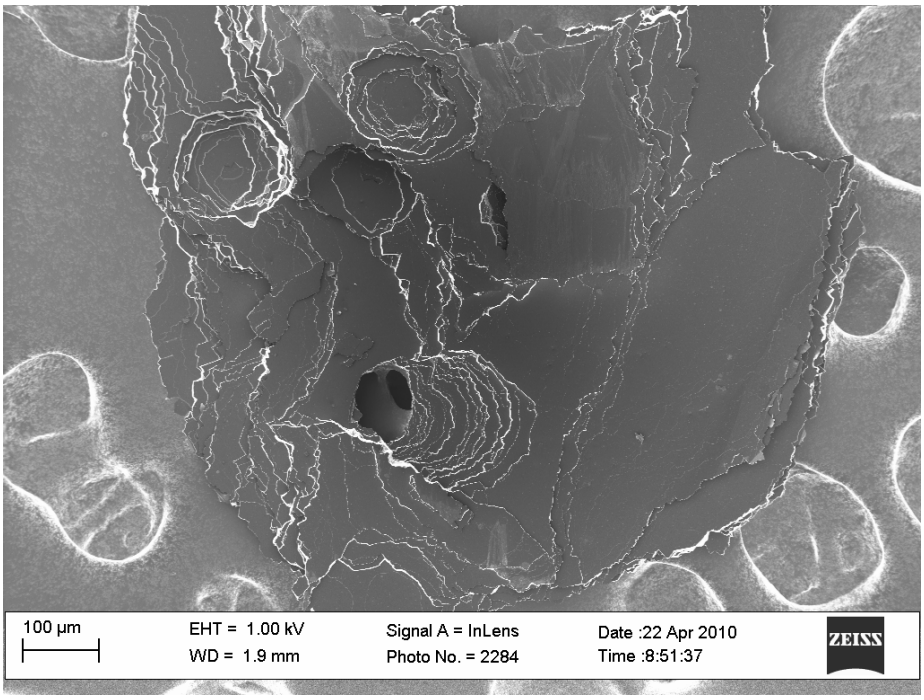

Figure 4-27: Oxidised Kish graphite flake (10 000x magnification)

These pits are presumably initiated at lattice defects and are distributed randomly across the flake surface. They affect the development of the active surface area in a complex manner and this effect will differ from one particle to the next. Since it is impossible to obtain a set of identical flakes with identical surface area development, a compromise is necessary. A reasonable amount of sample consisting of fairly large flakes will lead to an averaging effect. Thus despite the variations in shape and structure from particle to particle, the sample will behave in a similar fashion during each experiment.

Ideally, the sample should contain large, highly crystalline flakes since such a particle would be fairly easy to model. If the flakes are large, they have a low specific active surface area and the bulk sample will have ample void space. These factors are critical to ensure the absence of mass transfer limitations within the sample. The as-received RFL graphite material is shown in Figure 4-28. The sample contains a variety of particle sizes so the material was wet sieved in ethanol and only the 200–250 µm fraction was retained.

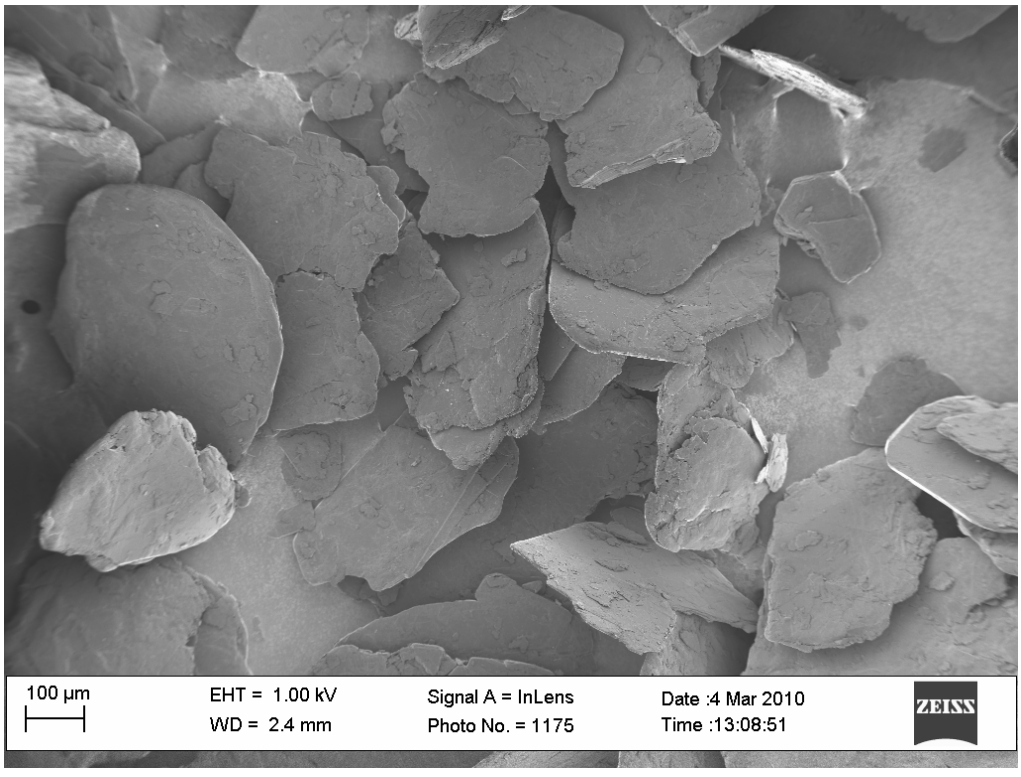

Figure 4-28: SEM of as-received RFL graphite (175x magnification)

From this point on, when referring to the RFL graphite, it will be implied that the material was sieved as described. The size fraction retained is shown in Figure 4-29. As can be seen from this figure, the sample contains large, thin, flat flakes.

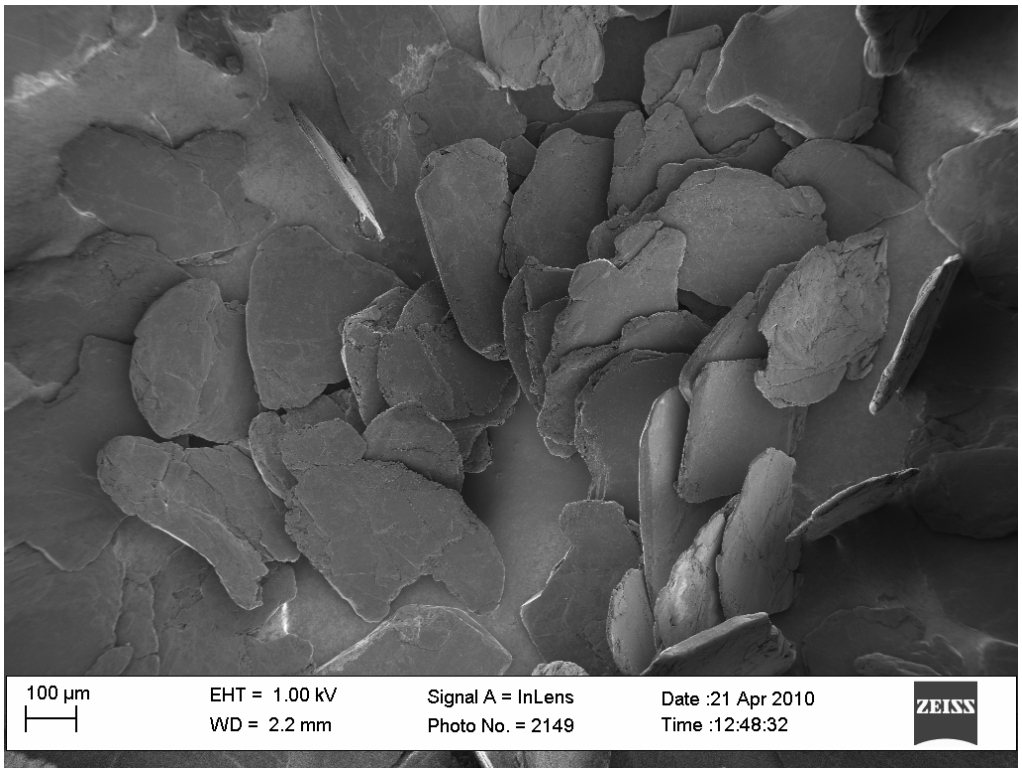

Figure 4-29: SEM of sieved RFL graphite (150x magnification)

Upon closer inspection, the characteristic layered graphitic nature of the flakes is readily visible, as can be seen in Figure 4-30. In general, the flake edges show minimal damage. When the sample is oxidised, the basal plane remains intact across virtually the entire flake, indicating a very high degree of crystallinity throughout, as shown in Figure 4-31. Furthermore, examination of the edges shown in Figure 4-32 shows that they are oxidised fairly smoothly, indicating large domains in the c-direction. However, the activity of catalytic particles is immediately evident throughout, visible mainly as erratic channelling. In addition, the presence of large fissures that cut across the flake surface are noticeable when the flakes are oxidised, as can be seen in Figure 4-33 and Figure 4-34.

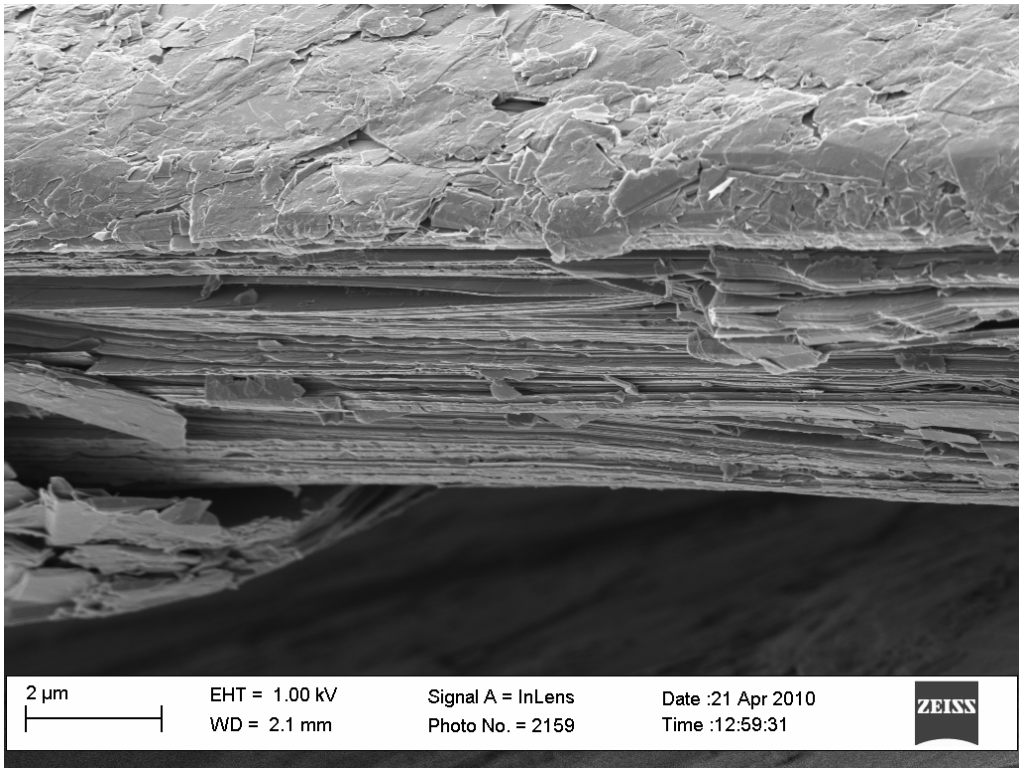

Figure 4-30: SEM of RFL flake edge (20 000x magnification)

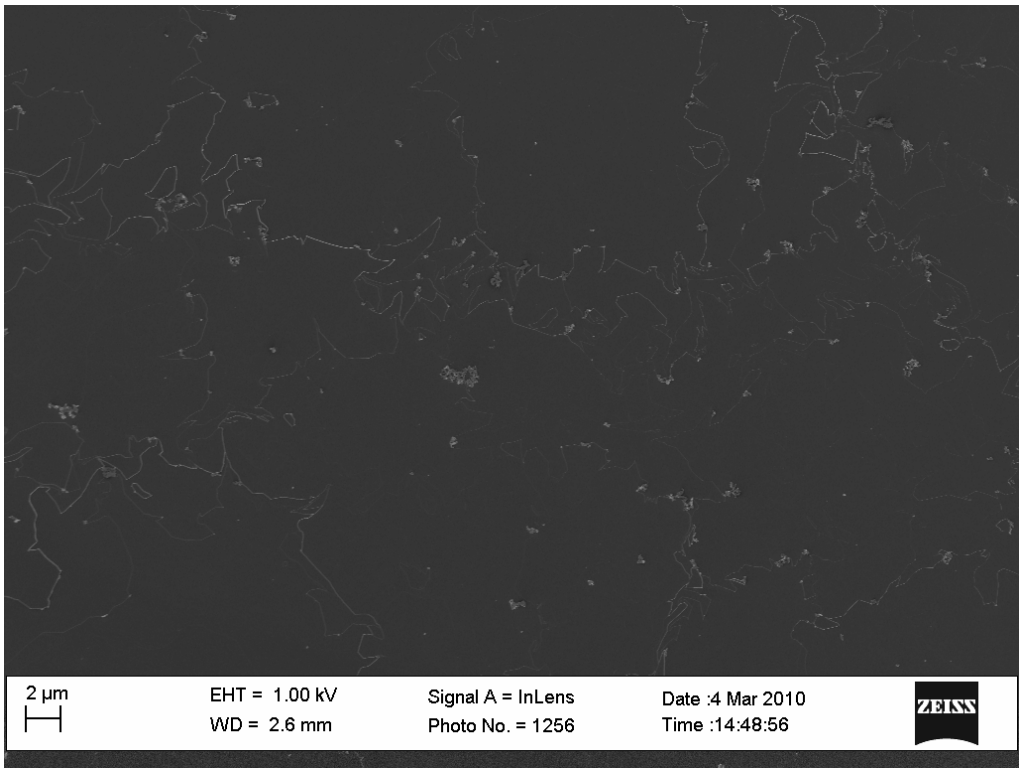

Figure 4-31: SEM of oxidised RFL flake basal plane (5 000x magnification)

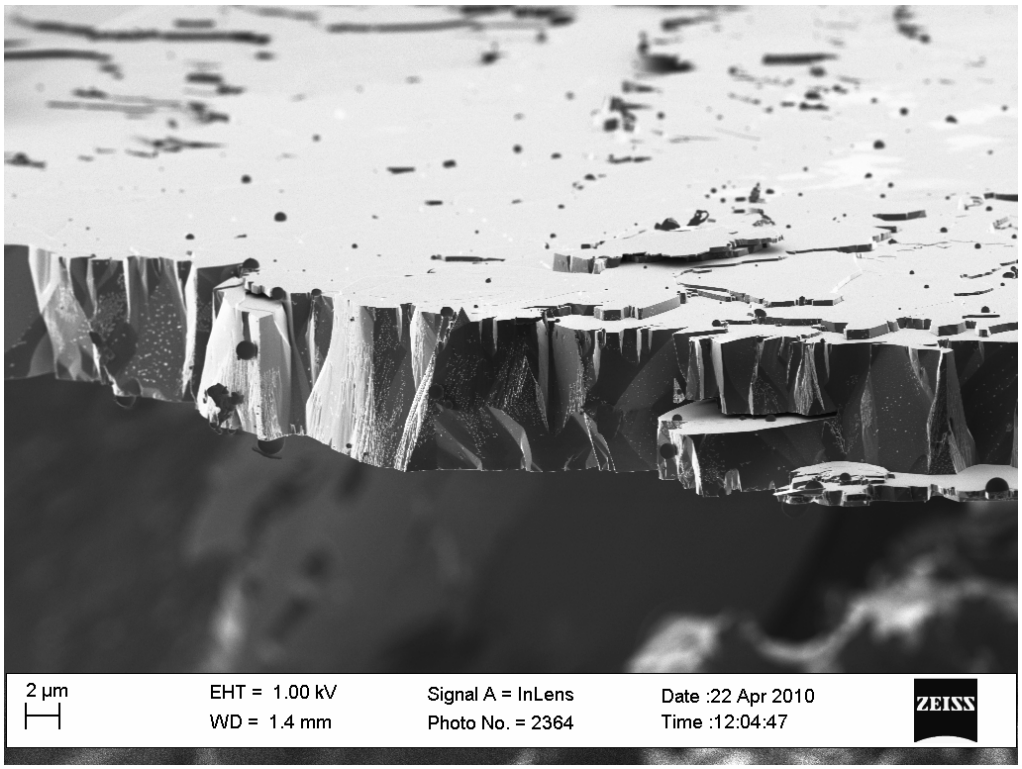

Figure 4-32: SEM of oxidised RFL flake edge (5 000x magnification)

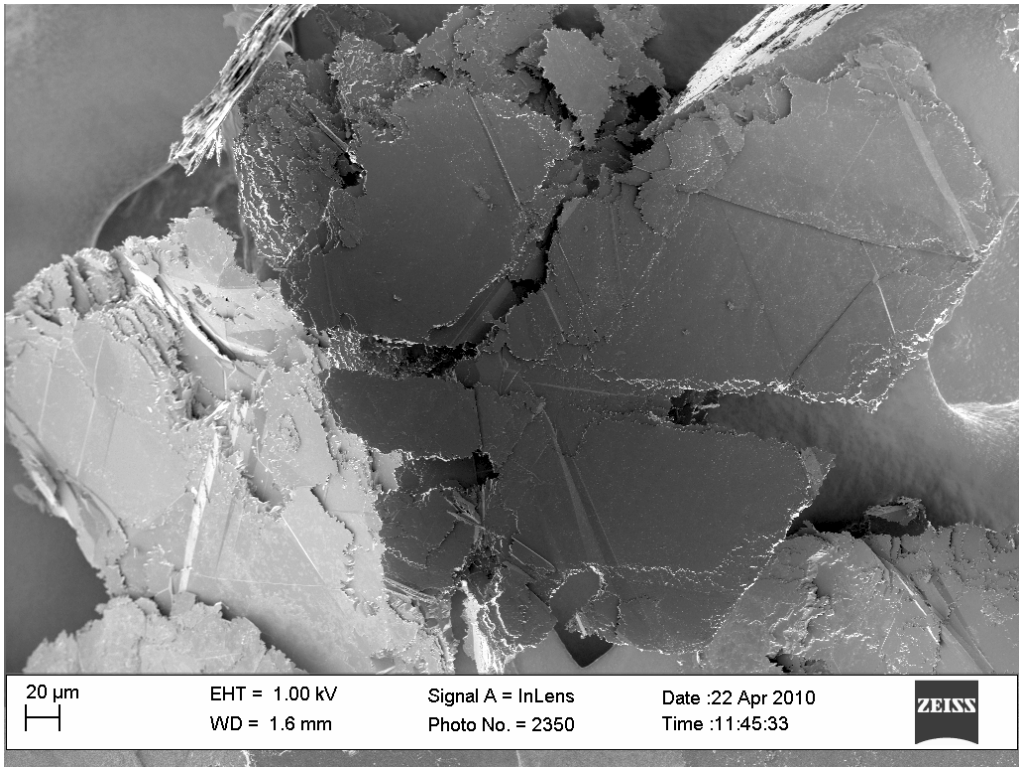

Figure 4-33: SEM of oxidised RFL flake with fissures (500x magnification)

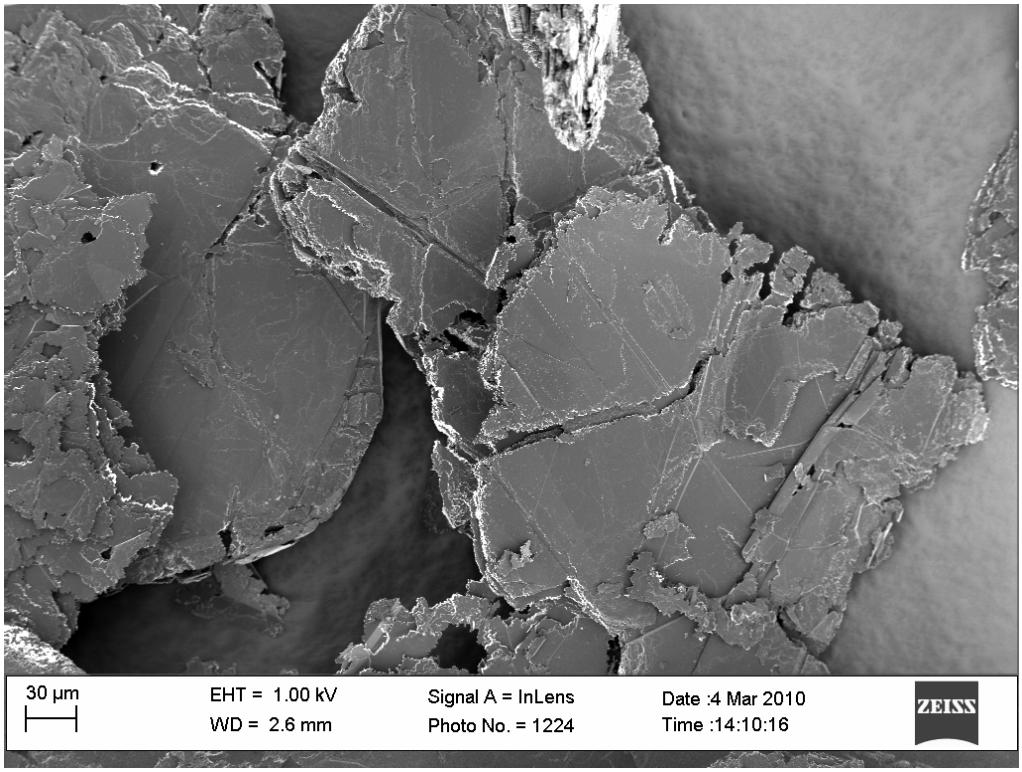

Figure 4-34: SEM of oxidised RFL flake with fissures (1 000x magnification)

In addition to the fissure structures within the more or less macroscopically intact flakes, a variety of other microstructures are readily observable, such as the highly pitted structure shown in Figure 4-35. More erratic and complex microstructures are also distinguishable, such as the example shown in Figure 4-36.

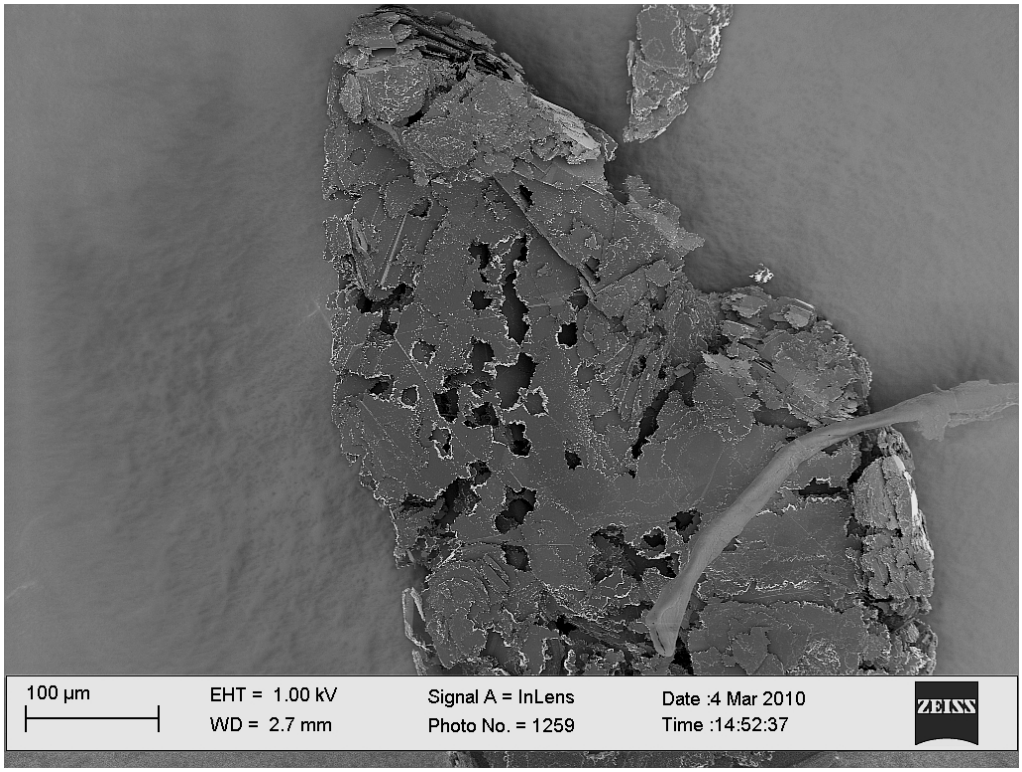

Figure 4-35: SEM of oxidised RFL flake with pits (390x magnification)

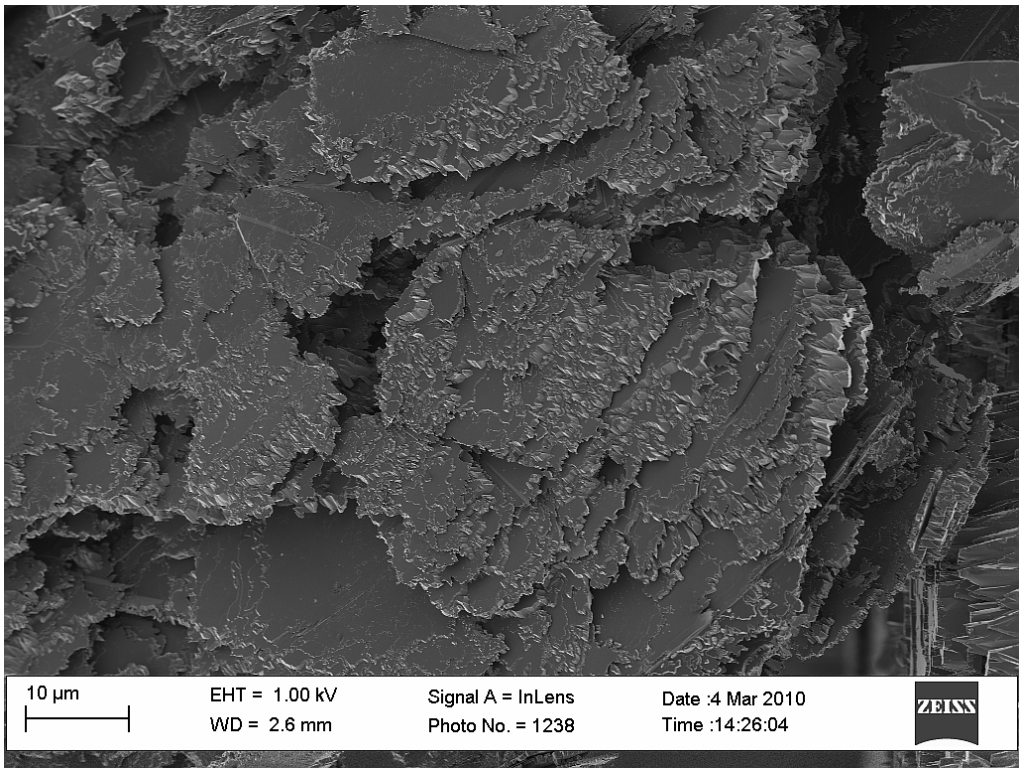

Figure 4-36: SEM of oxidised RFL flake with erratic and complex structure (3 000x magnification)

The final sample to be considered in this section is the fully purified RFL graphite. As a preface, it is worthwhile to consider two images of the partially purified material. In Figure 4-37 the channelling actions of individual catalyst particles are clearly visible. Furthermore, when the tips of these channels are examined more closely, as in Figure 4-38, it is possible to discern an individual catalyst particle less than 10 nm in diameter. This serves to illustrate the resolving capability of the SEM used to inspect the graphite samples. It lends credence to the statement that if no microscopic channels are visible and no individual catalyst particles are discernible under SEM examination, it is safe to conclude that there is no catalytic activity in the sample. However, the presence of pitting catalysts is still possible.

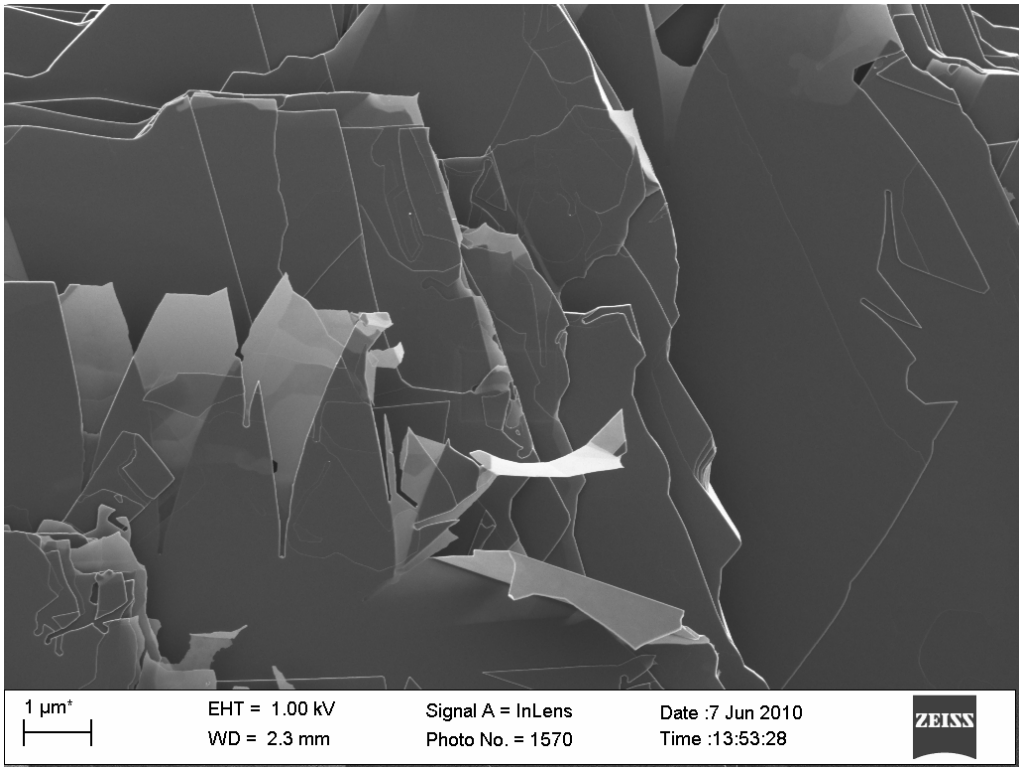

Figure 4-37: SEM of a partially purified RFL flake (20 000x magnification)

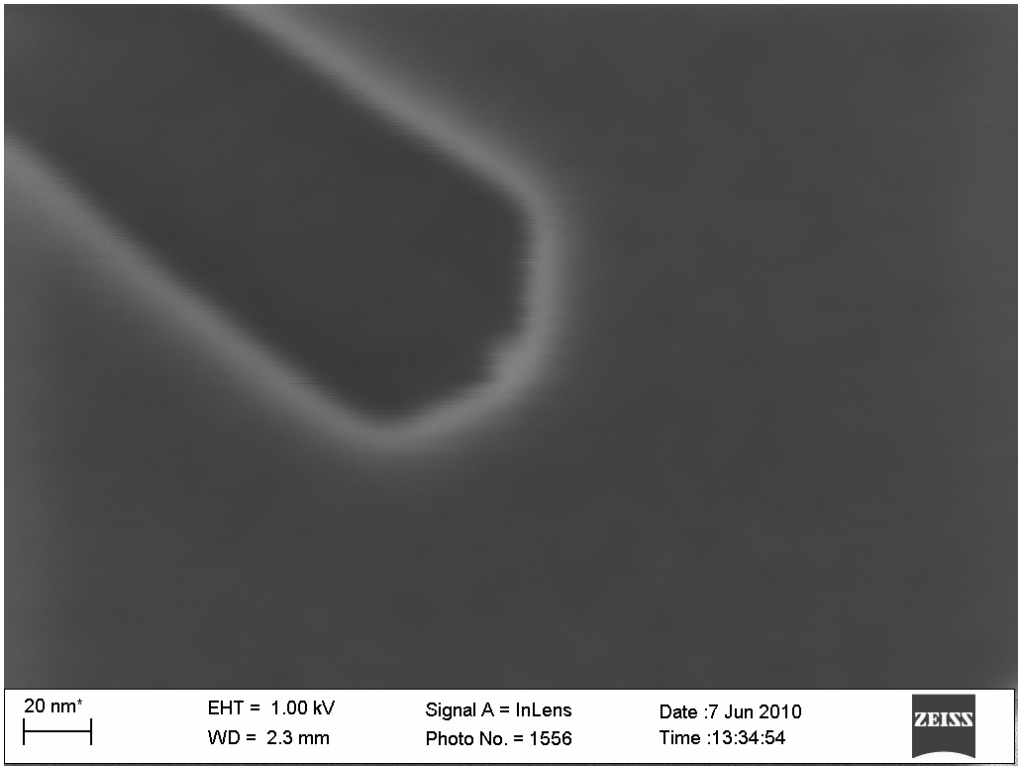

Figure 4-38: SEM of a catalyst particle (1 000 000x magnification)

The purified RFL samples were extensively scrutinised and no channelling phenomena or catalyst particles were observed, even at very high magnifications. Instead, the oxidised particles consistently developed flat edges with characteristic 120º angles, as can be seen in Figure 4-39 and Figure 4-40. Furthermore, the basal planes of the oxidised flakes remain virtually untouched, as can be seen in Figure 4-41. This indicates that a homogeneously dispersed pitting catalyst is not present. This is further substantiated by recalling the fact that when these samples were not cooled at a very slow cooling rate, extensive pitting was observed, indicating that the few remaining instances of pitting are due mainly to lattice defects.

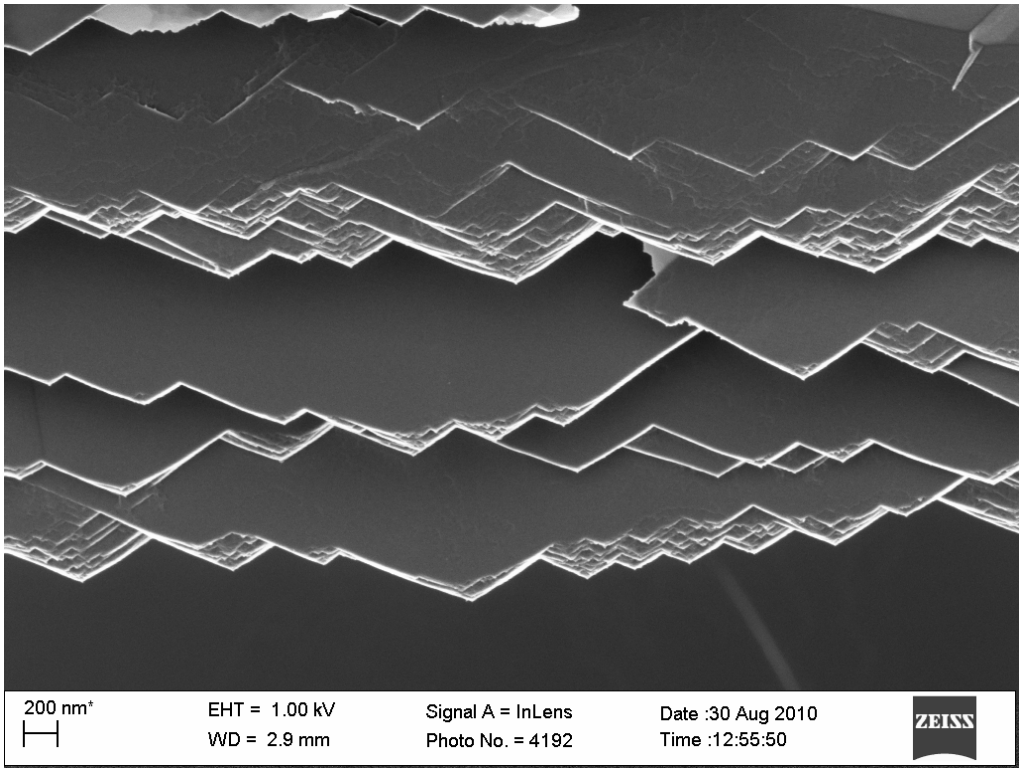

Figure 4-39: SEM of oxidised purified RFL flake edge (20 000x magnification)

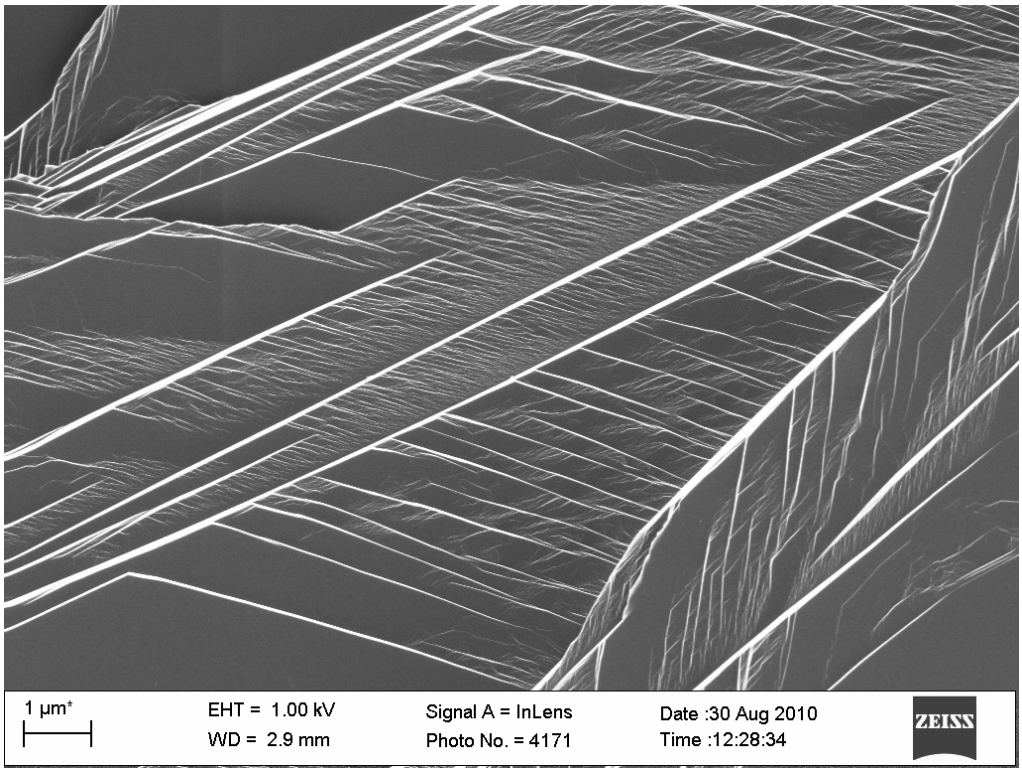

Figure 4-40: Purified and oxidised RFL flake edge (20 000x magnification)

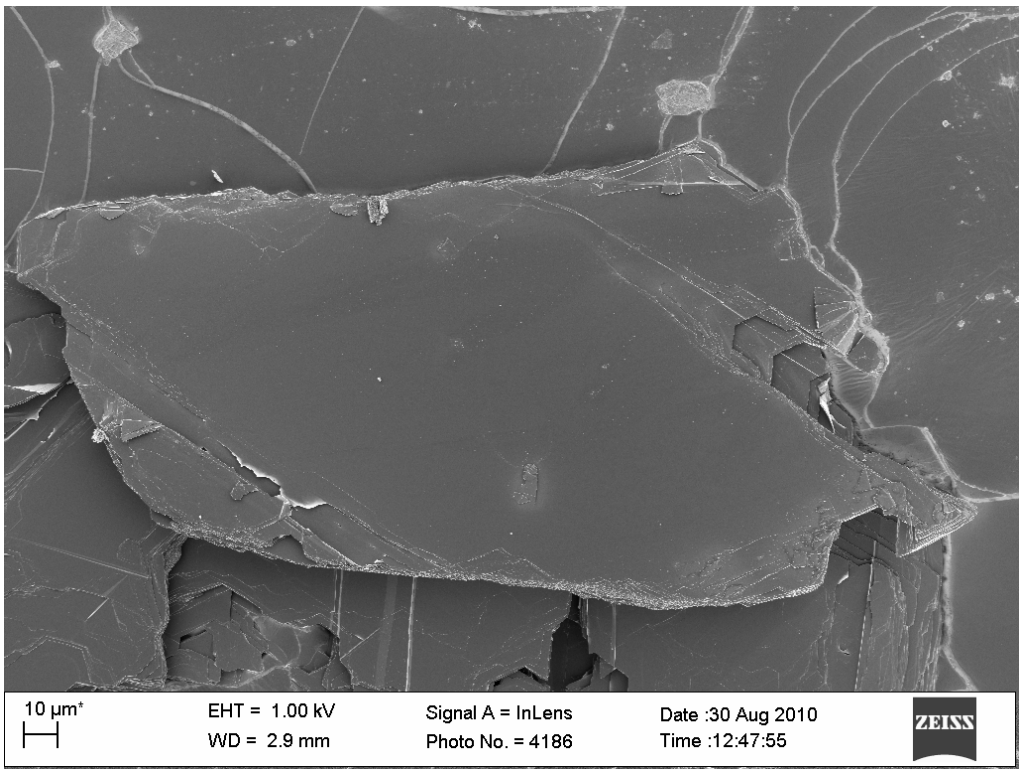

Figure 4-41: Purified and oxidised RFL flake basal plane (100x magnification)

It is highly unlikely that such a short heat treatment modified the medium- to long-range atomic ordering of the graphite. These observations therefore confirm the assertion that the original RFL material is highly crystalline. When the unoxidised purified flakes are examined, a few key microstructural elements are discernible which strengthen the previous statement. The presence of islands or protrusions on the basal surface can be seen in Figure 4-42. These structures bear a remarkable resemblance to the morphology of the single-crystal graphite samples studied by Palache [344]. When examined more closely, their layered construction is clearly evident, as in Figure 4-43.

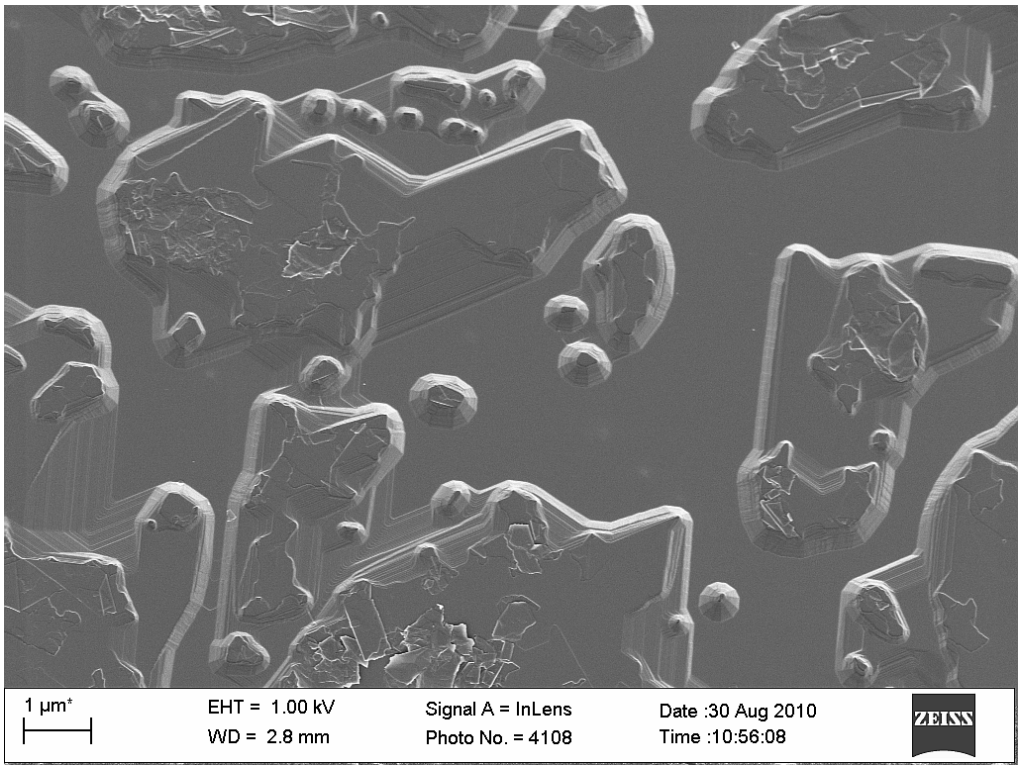

Figure 4-42: Basal structures on purified RFL flake (20 000x magnification)

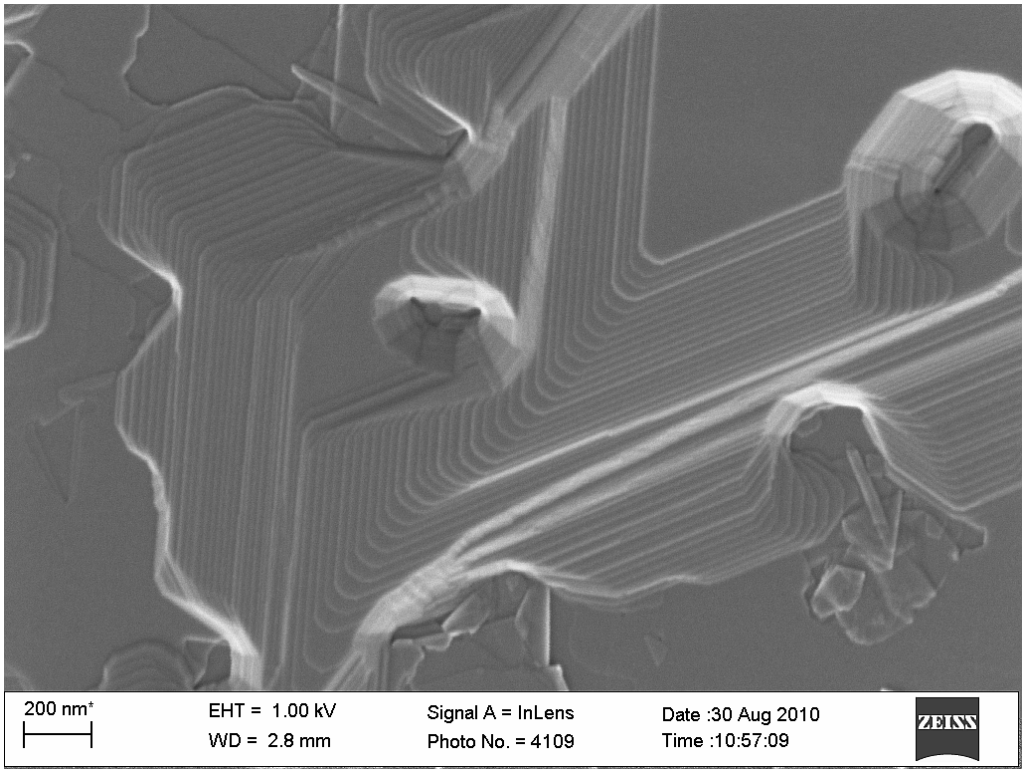

Figure 4-43: Layered nature of RFL basal structures (100 000x magnification)

This is consistent with the notion that these are perfect graphite crystals, which formed with inclusions of other minerals. As the graphitic layers grew, some of the natural minerals present were trapped in the graphite crystal structure. Upon heating to high temperature, these impurities were evaporated to leave behind the true graphite crystal structure. In some cases large fissures, similar to those observed for the oxidised as-received flakes, are noticeable, for example in Figure 4-44. When the walls of these structures are examined, a similar layered texture is visible, as in Figure 4-45.

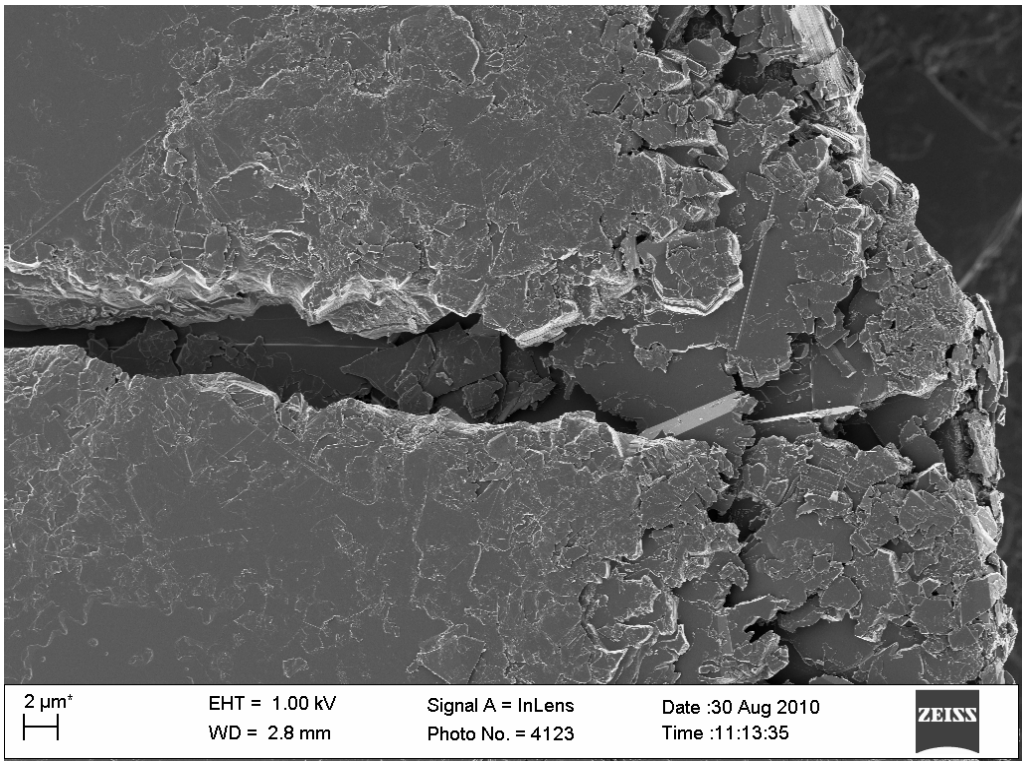

Figure 4-44: Fissure in purified RFL graphite (5 000x magnification)

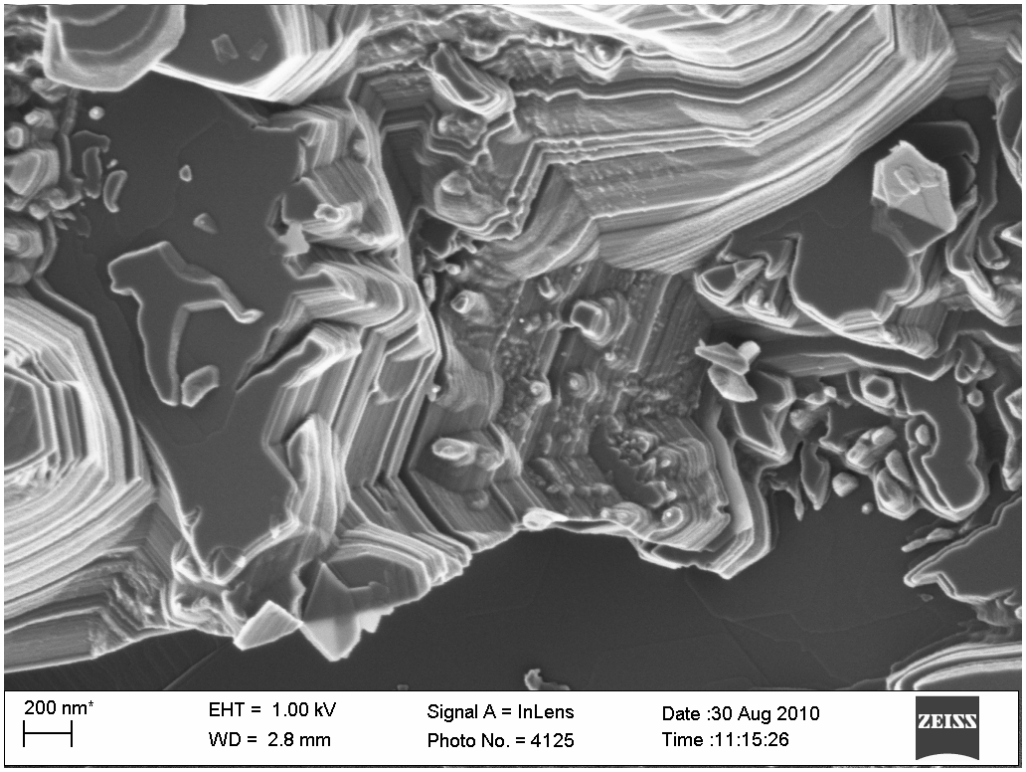

Figure 4-45: Layered texture of fissure wall (5 000x magnification)

It was concluded that the fissures are, in fact, large mineral inclusions, which were formed when the graphite crystal originally precipitated. When the flake is oxidised, the area adjacent to the impurity is a free edge site and open to attack. Hence oxidation proceeds from this point and the fissure becomes visible within the macrostructure of the flake.

It is interesting to note that, in addition, the layered inclusion structures are also present as a fine microstructure on the flake surface, as can be seen from Figure 4-46.

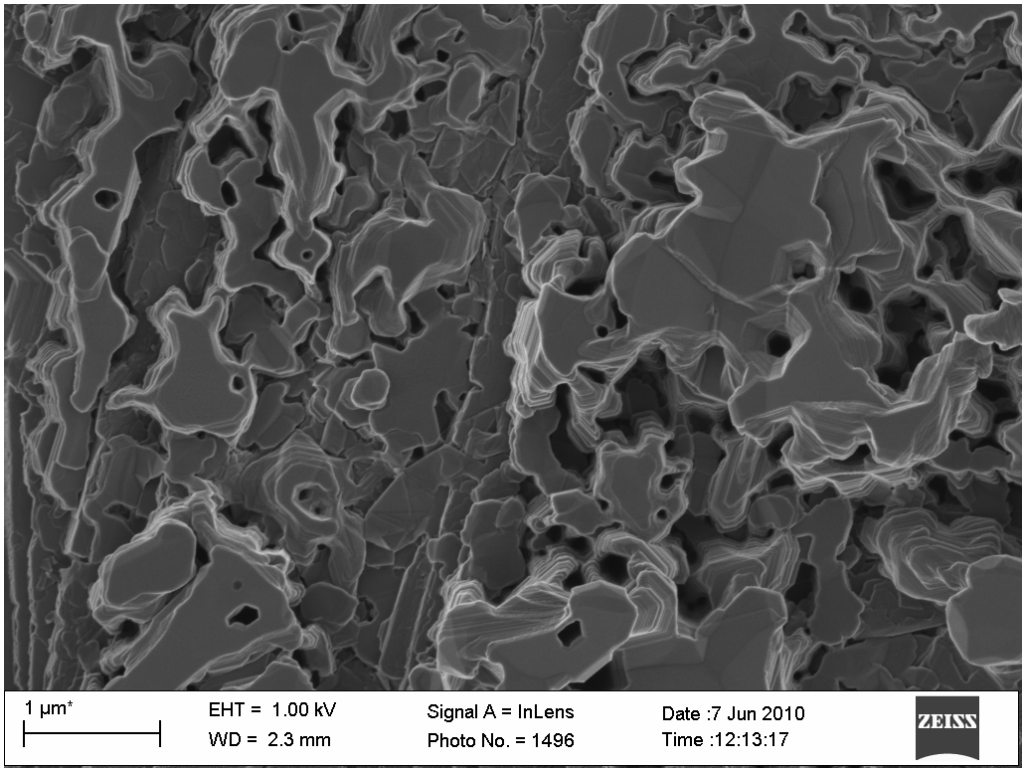

Figure 4-46: Fine texture of surface inclusions (40 000x magnification)

The structures do not appear to penetrate deeply into the flake body. Thus during oxidation these represent regions of high reactivity due to a high active site area concentration. Such areas would be rapidly oxidised to leave behind the macrobody of the flake; an example of this is shown in Figure 4-47.

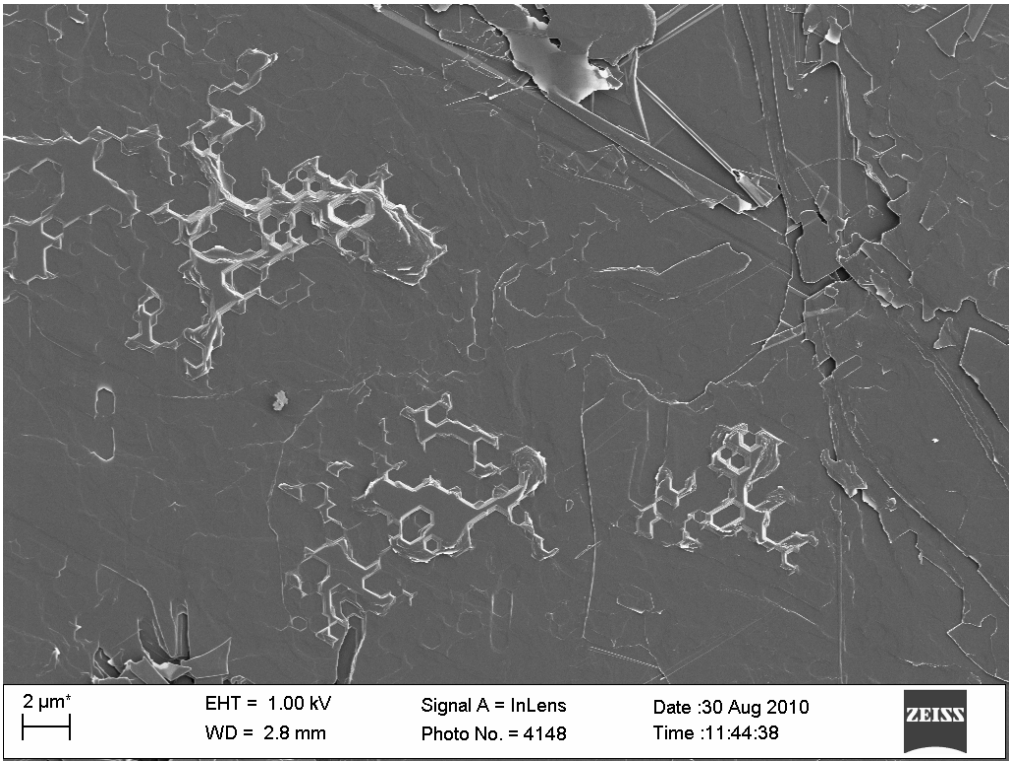

Figure 4-47: Oxidation of fine surface structures (7 000x magnification)

Thus of all the graphite samples considered, the RFL material shows the most promise as a model material for investigating the mechanisms that govern the oxidation of graphite since this material appears to be highly crystalline, having a consistent flake-like structure and a large particle size.